MESONIC SOURCES OF DILEPTONS

IN ULTRARELATIVISTIC NUCLEAR COLLISIONS

Ioulia Kvasnikova

Physics Department

McGill University

Montréal

January 26, 2001

A thesis submitted to the Faculty of Graduate Studies and Research
in partial fulfillment of the requirements
for the degree of Doctor of Philosophy.

0-612-70069-0

Abstract

In this work thermal dilepton production from a hot medium created in heavy ion collision is studied. Using an effective Lagrangian technique for particle decays and annihilations, a complete method for calculation of the lepton pair production rate is developed. The importance of axial vector meson contributions to the dilepton spectrum is analyzed. Different effective Lagrangians for the $a_1\rho\pi$ interaction are considered, and a new form of $b_1\omega(\phi)\pi$ effective Lagrangian is introduced.

A systematic study of light meson contributions is performed. The most significant decay and reaction contributions are calculated and summed for low and intermediate invariant mass dileptons. The calculated dilepton rate is compared to that obtained using spectral functions extracted from data, and it is shown that the chosen set of mesonic reactions and decays accounts for all significant contributions to the thermal dilepton emission.

A hydrodynamic approach to the space-time evolution of the hot medium formed as a result of a central heavy ion collision at ultra-relativistic energies is considered. A theoretical curve of intermediate invariant mass dilepton spectrum is computed and compared to the NA50 data from central Pb(158 AGeV)+Pb collisions. Experimental acceptance cuts are accounted for. Drell-Yan processes are considered as well. We find that our thermal dileptons account for the intermediate mass excess observed by the NA50 Collaboration. We see no need to invoke charm enhancement. Predictions for the future experiments at RHIC and are made.

Résumé

Dans cette thése, nous étudions la production de paires de leptons dans les collisions d'ions lourds. Avec une approche basée sur les Lagrangiens effectifs, nous établissons une méthode pour le calcul des taux d'émission. L'importance des pseudo-vectors est soulignée. Plusieurs Lagrangiens effectifs pour l'interaction $a_1\rho\pi$ sont considérés et nous présentons un nouveau Lagrangien pour l'interaction $b_1\omega(\phi)\pi$.

Nous faisons une étude systématique des contributions des mésons légers, en soulignant les canaux importants dans les régions de basse et de moyenne masse invariante. Les taux de dileptons sont comparés à ceux obtenus avec des fonctions spectrales expérimentales. Nos canaux choisis saturent celles-ci.

L'evolution temporelle est traitée avec un modèle hydrodynamique. Nous comparons nos spectres de dileptons de masse moyenne avec ceux mesurés par NA50. Nos contributions thermiques reproduisent bien l'excès mesuré par NA50. Nous faisons finalement des prédictions pour RHIC.

Aknowledgments

It is my deep pleasure to thank all the people who helped me during the preparation of this thesis.

I would like to express my sincere gratidude to my superviser Prof. Charles Gale, whose continious guiding, support and valuable suggestions made this work possible, and whose sence of humor and patience helped to complete it.

The work here presented has been developed at Physics Department of McGill University. I am deeply thankful to all members and staff for valuable discussions and advices at different stages of the thesis preparation, for providing me with the computer support, for their sympathy and constant practical help.

I am specially grateful to Prof. D. K. Srivastava, whose collaboration at the late stages of work resulted in the research devoted to hydrodynamic model applications to heavy ion collisions.

I'd like to thank Ralf Rapp and Kevin Haglin for helping me to understand some aspects of finite temperature field theory.

I also wish to thank Slava Ispolatov for especially helpful criticisms and for rectifying errors in the manuscript.

Contents

Chapter 1

Introduction – Heavy ion collisions as a source of quark-gluon plasma

The most important and challenging goal of contemporary ultra-relativistic heavy-ion collision research is producing a new state of matter: quark-gluon plasma (QGP), in the laboratory. According to current theoretical predictions [1], creation of this new phase requires attaining extremely high temperature and/or density in a collision volume. Threshold energy density is comparable to that in neutron stars [1]. Ultra-relativistic Heavy Ion Colliders can explore this regime. Two machines that are currently in operation, the Relativistic Heavy-Ion Collider (RHIC) at the Brookhaven National Laboratory and the CERN Super Proton Synchrotron (SPS), can produce media with sufficient densities and temperatures. Soon, the Large Hadron Collider (LHC) at CERN will continue the heavy ion program at even higher energies.

A typical space-time diagram for the ultra-relativistic nucleus-nucleus collision is shown in Figure 1.1 Created in central collisions of heavy nuclei at ultra-relativistic

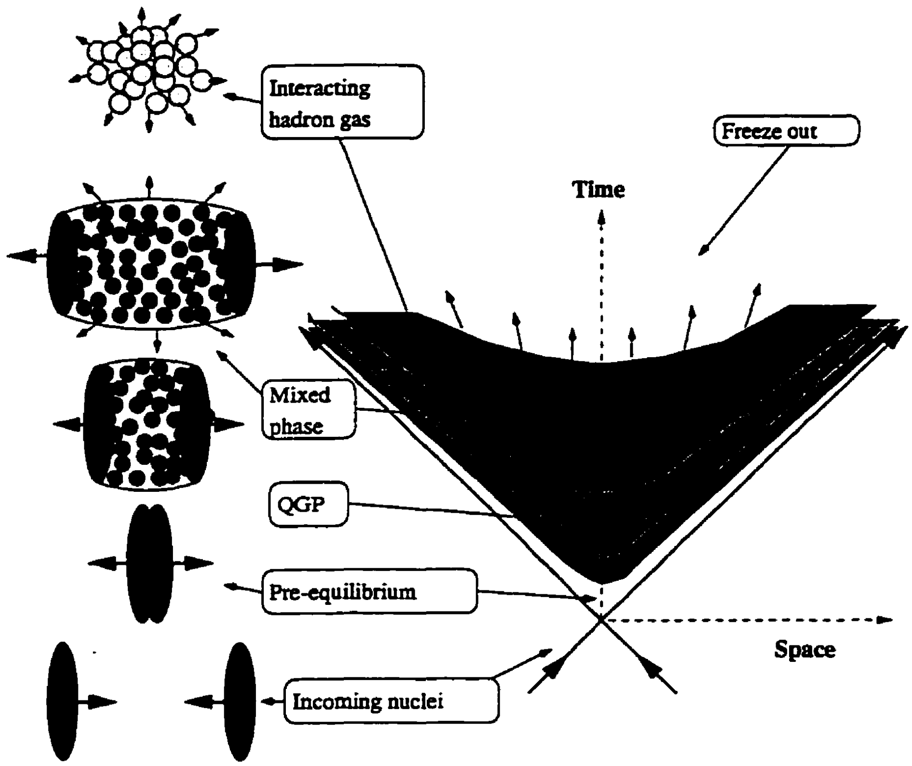

Figure 1.1: Space-time diagram for nucleus-nucleus collision, showing the various stages of the evolution of the expanding matter.

energies (up to $\sqrt{s}$=0.2-10 ATeV at RHIC and LHC), hot and dense hadronic matter may exist over extended period of time (up to 20 fm/c). Within the first fm/c, the system reaches local thermal equilibrium, after which the "fireball" expands and cools until the strong interactions decouple (or undergo "thermal freeze-out") [2]. Electromagnetic radiation (real and virtual photons and dileptons) is continuously emitted during the existence of the fireball since its reabsorption by the strongly interacting matter is negligible.

What is the transition temperature to this new state?

Lattice QCD calculations give values between 140 and 180 MeV which corresponds to an energy density of about 1 GeV/fm^3, or 6-7 times that of nuclear matter [3]. Specifically, at zero baryon density the critical temperature is about 170 MeV [4]. A theoretical analysis of the measured hadron abundances [5-8] shows that the fireball reaches a state of "chemical equilibrium" at 170-190 MeV. A recent analysis [9] yields a value of 181.3$\pm$10.3 MeV for the chemical freeze out temperature.

It is natural to ask the question of how one can probe whether the phase transition of hadrons into a plasma of deconfined quarks and gluons actually takes place in ultrarelativistic heavy ion collisions. There are some reasons that make it difficult to detect QGP directly. If created, the QGP state would have rapidly fading existence. Due to the color confinement single quarks and gluons will be forced to hadronize. Thus, at later times the collision fireball turns into a system of hadrons, regardless of whether or not QGP is formed in the initial stage. In a head-on Pb-Pb collision at the CERN SPS about 2500 particles are created [10], more than 99.9 % of them are hadrons, the remaining ones are leptons and photons. Evidence for deconfined quarks and gluons formation can only be based on a multitude of different observations and has to be extracted by a careful and quantitative analysis of the observed final state. Therefore possible evidence for QGP formation, if any, is indirect, as it is extracted from the measurement of particles which have undergone significant reinteractions between the early collision stages and their final detection. Still, they may retain enough memory of the initial quark-gluon state to reveal its possible existence. Electromagnetic signals which are emitted directly from the quarks in the QGP and escape later interaction may constitute a source of more direct information.

Let us identify some specific signatures that can be used to probe the phase transition between hot hadronic matter and a quark-gluon plasma, and to study the characteristic properties of the latter. First of all, heavy vector mesons, especially the charmonium states J/ψ, are excellent indicators of color deconfinement. It is predicted [11] that J/ψ production is strongly suppressed if a QGP is formed. Secondly, the proximity of chiral symmetry restoration can be probed by possible corresponding shifts in masses and widths of light vector mesons, which may be detected via their lepton-pair decays [12]. Another evidence for a possible phase transition is an enhanced yield of multistrange baryons and antibaryons that is expected due to a high gluon content of the QGP [13]. Finally, direct photons and thermal lepton pairs can be used to probe the interior of the QGP [14]. Their spectra and yields track the thermal history of the dense matter and should provide information about the temperature and duration of the mixed phase.

An excess of dileptons in the low invariant mass region between 250 and 700 MeV has been revealed [7, 8]. The ratio of the measured yield over the expected one from hadron decays scaled from proton-nucleus (p-A) collisions is about 3. The enhancement is concentrated at low pair transverse momentum [15]. Among suggested explanations of such enhancement [17] is the broadening of the ρ's spectral function, resulting from scattering in the medium with its hadronic constituents. Another scenario is that of the dropping meson masses, as a precursor to chiral symmetry restoration [18, 19]. Before those explanations can be made viable, a complete study with vacuum properties is needed. This is our goal in this work. Experimental measurements [7] show that in intermediate mass region in S-Au and Pb-Au collisions the expected peak from the ρ vector meson, which can decay into dileptons even before the freeze-out, is completely washed out. Being a good source of information about formation of a quark-gluon plasma [16], this experimental data makes it of our particular interest to investigate possible sources of such behavior in the low and intermediate invariant mass region. Dileptons may indicate the appearance of a QGP phase, in particular at RHIC and LHC [22].

Direct observation of the QGP may thus be possible via electromagnetic radiation emitted by the quark-antiquark pairs during the hot initial stage. Search for these signals was performed at the SPS [5, 6, 7] but this task is rather difficult to accomplish due to the existence of other contributions from the confined hadronic sector. Also, the predicted electromagnetic radiation rates at the temperatures close to critical are marginal for detection. That is possibly why the predicted "thermal plasma radiation" has not been firmly confirmed yet. Also, from an experimentalist point of view, the measurements are very challenging.

The significant enhancement of the dilepton spectrum measured in nucleus-nucleus (A-A) collision as compared with proton-nucleus (p-A) collisions indicate also the appearance of collective phenomena, such as rescattering of secondaries, in the created medium. For hadronic phase, the reactions involving light mesons (pions, ρ-mesons etc.) are also important and have to be included into consideration. Many theoretical efforts (see, for example, Ref. [23]) have concentrated on the role of medium effects in the fireball created at the hadronic stages of ultrarelativistic heavy ion collisions as the interacting mesons in the fireball are the significant source of electromagnetic radiation.

In this work we are concerned with interactions of light mesons in a hot baryon-free system resulting in dilepton emission. For the purposes of theoretical analysis, the dilepton mass spectrum is roughly subdivided in three main regions: the Low Mass Region (LMR) below the ϕ resonance, the Intermediate Mass Region (IMR) between the ϕ and the J/ψ and the High Mass Region (HMR) above the J/ψ. The main goal of our research is to obtain the differential rate of thermal dilepton production from the hot and dense collision fireball in the intermediate (IMR) invariant mass region, where QGP is expected [16, 24]. The main strategy is based on employing as much the experimental data as possible. In other words, everything we do is immediately compared to, and constrained by, the experimental information at hand.

The fact that effective theories in the confined sector of QCD cannot be specified uniquely immediately implies that one must examine carefully the models that are available. In Chapter 2 we start with a revision of effective Lagrangians of mesonic interactions. Then we explore various theoretical and mathematical approaches to the dilepton emission rate calculations in the most general way and specify the details of our particular technique. We talk qualitatively about the formalism that we use, relativistic kinetic theory, and its advantages compared to the finite temperature field theory method.

In Chapter 3, we consider different interaction Lagrangians for the case of a_1 interaction. It is of interest to consider dilepton production through a_1 resonance since a_1 has been known to be very important in photon production [25]. We talk about general phenomenology of hadronic interactions, calculate the width of radiative and strong decays, D/S ratio, as well as the differential dilepton production rate. After comparison of the obtained quantities to the available experimental data, the choice of the optimal interaction Lagrangian is justified. We also introduce a new form of Lagrangian for $b_1\omega\pi$ interaction and justify our choice.

Chapter 4 is devoted to the particular meson contributions in the LMR and IMR regions. We calculate differential rates of the dilepton production for a number of contributing reactions using various constraints extracted from the experimental data. To our knowledge, it is the most complete list of mesonic contributions to the thermal dilepton production in heavy ion collisions. We want to check quantitatively the applicability of the suggested approach to our invariant mass region of interest. For this purpose we compare the result to the data obtained using the collection of spectral functions which are extracted from e^+e^- annihilation and τ lepton decay data [26] in

LMR and IMR. As a result of the comparison we claim that the selected set of chosen mesonic reactions and decays is indeed the collection of the leading contributions to the thermal dilepton emission. Once having established that, we turn to IMR where the signals of quark-gluon plasma formation are expected.

We apply the results of the calculations to the rate evaluation using realistic hydrodynamic model of heavy ion collisions. This model is implemented in Chapter 5. There, we discuss possible sources of dileptons in the intermediate mass region and calculate differential rates of thermal lepton pairs and Drell-Yan process contributions. The calculations are carried out within the assumption that the first order phase transition from the quark to the hadron phase actually takes place. We compare our theoretical results to the experiment. For this purpose the acceptance cuts are implemented and calculated. The predictions for future experiments are also carried out.

All our results and conclusions are summarized in last Chapter.

Chapter 2

Theory of mesonic interaction in a hot hadronic matter

In this chapter we review the theory of effective Lagrangians for meson interactions and justify choosing it for our case of study. We explore the theoretical and mathematical approaches to the dilepton emission rate calculations in the most general way and specify the details of our particular technique. We talk qualitatively about the formalism that we use, relativistic kinetic theory, and its advantages compared to the finite temperature field theory methods. We develop a complete method for lepton pair production rate calculation given an interaction Lagrangian involving the meson fields.

2.1 General remarks on the origin of effective Lagrangian

Our starting point is an ensemble of mesons in thermal equilibrium. It is clear that at some temperature one would have a gas of the lightest hadrons from the nonet of light pseudoscalar mesons. For such temperatures the hadronic matter can perhaps be approximated as a pion gas. As the gas becomes more dense, one should include into consideration vector and axial-vector mesons and take into account interaction among them. In order not to restrict ourselves to any thermal limitations, we will consider all possible light resonances. At a later time for a sake of simplicity we will rule out the unimportant and irrelevant ones.

Even though there is no concrete theoretical technique today to study intermediate energy hadronic matter from first principles, some experimental data are available which could help us to understand the nature of hadronic interactions. It is convenient to treat the mesons in hadronic matter as the elementary fields using an effective Lagrangian, which is constructed from symmetries and the anomaly structure of the fundamental theory, QCD. However, there are parameters in the Lagrangian that cannot be determined from the fundamental theory but must be inferred from the experimental data. In a certain sense, the theory and the experiment are combined in the determination of an effective Lagrangian.

The lowest order interaction in the interacting fields that we will need corresponds to the three-point function. This comes out of effective chiral theories [27, 28]. The three-point vertices will dominate the dynamics we are concerned with here. We thus can expand

$$\mathcal{L} = \mathcal{L}_{VPP} + \mathcal{L}_{VAP} + \mathcal{L}_{VVV} + \mathcal{L}_{VVP} \quad (2.1)$$

Here letters V, A, ϕ stand for vector, axial-vector and pseudoscalar meson correspondingly. All other possible permutations are ruled out because of symmetry and conservation law considerations. We include into consideration the anomalous interaction VVP which is obtained from the Wess-Zumino term.

2.2 Vector Meson Dominance Model

Presence of vector meson as participating in the reaction particle is crucial for dilepton production. In the framework of Vector Meson Dominance Model (VMD) it transforms into a photon. This model, proposed by Nambu and developed by Sakurai [29], states that the photon interacts with physical hadrons through vector mesons. Hence, the hadronic electromagnetic current operator is given by the following *current-field identity*:

$$J_\mu = -\frac{e}{g_\rho} m_\rho^2 \rho_\mu - \frac{e}{g_\phi} m_\phi^2 \phi_\mu - \frac{e}{g_\omega} m_\omega^2 \omega_\mu. \quad (2.2)$$

In practice it means that the neutral component of the hadronic vector field $V^{I_3=0}$ couples directly to the photon A^μ via [29]

$$\mathcal{L}_{VA} = (\frac{em_V^2}{g_V})V_\mu^{I_3=0}A^\mu \qquad (2.3)$$

For the energy and dilepton invariant mass range considered here, the lightest vector mesons will be the dominant vector fields. In invariant mass regions where heavier vector mesons come into play, we use an experimentally determined form factor.

2.3 Discussion on a choice of effective Lagrangian

Now, once we have established the introductory part of our model, we need to describe how the mesons interact among themselves. Let us start with a simple phenomenological approach, inspired by the chiral properties of QCD at intermediate energy and compatible with electromagnetic current conservation. So far, let us define the interaction as in Ref. [25] and Ref. [30] correspondingly

$$\mathcal{L}_{VPA} = G_{VPA}\, a_\mu(g^{\mu\nu}q\cdot p - q^\mu p^\nu)V_\nu P, \qquad (2.4)$$

$$\mathcal{L}_{VPP'} = G_{VPP'}\, V^\mu P\, \overleftrightarrow{\partial}_\mu P'. \qquad (2.5)$$

Here p^μ and q^μ denote the four-momentums of the pseudoscalar and vector mesons respectively, and G's are coupling constants representing the strength of interaction induced from hadronic experimental data.

The VVP interaction is determined by Wess-Zumino anomaly terms, which are of unnatural parity and involve the four dimensional antisymmetric Levi-Civita tensor $\epsilon_{\mu\nu\sigma\tau}$ [27]:

$$\mathcal{L}_{VV'P} = G_{VV'P}\, \epsilon_{\mu\nu\sigma\tau} k^{\mu} V^{\nu} q^{\sigma} V'^{\tau} P. \tag{2.6}$$

For VVV interaction we introduce the vector meson fields as a 3×3 nonet matrix [32]:

$$V = \begin{pmatrix} \frac{\rho^0}{\sqrt{2}} + \frac{\omega}{\sqrt{2}} & \rho^+ & K^{*+} \\ \rho^- & -\frac{\rho^0}{\sqrt{2}} + \frac{\omega}{\sqrt{2}} & K^{*0} \\ K^{*-} & \overline{K}^{*0} & \phi \end{pmatrix}. \tag{2.7}$$

In this case the interaction Lagrangian can be represented as

$$\mathcal{L}_{VVV} = \frac{i\, G_{VVV}}{2}\, Tr(\partial_{\mu} V_{\nu} - \partial_{\nu} V_{\mu})\, V^{\mu} V^{\nu}. \tag{2.8}$$

These effective interaction terms can be formalized in a chiral model [28]. After we have defined our effective meson Lagrangians we can proceed with possible approaches to the lepton pair emission rate calculations. There are two widely applied schemes to handle the mathematical formalism. We used relativistic kinetic theory that is a direct and intuitive formalism, but a few words need to be said about another method, that is finite temperature field theory. The qualitative comparison between these two approaches has indicated [34] that the finite temperature field theory technique has some apparent advantages over relativistic kinetic theory. First, the existence of a preferred thermal reference frame and broken Lorentz invariance can be identified through the separately resolved transverse and longitudinal parts of self-energy in finite temperature field theory [35]. Second, summation of different processes in self-energy formalism is done in such a natural way that interference effects are a lot easier to consider than in the relativistic kinetic theory approach.

But despite the sophistication and other formal advantages of finite temperature field theory approach, the results obtained using field theory formalism do not differ much from kinetic theory calculations if we restrict ourselves to a purely mesonic medium [35]. The finite temperature self-energy inserted into expression for the kinetic theory thermal rate of the e^+e^- production gives almost the same rates as in finite temperature formalism. The difference gets bigger as we go to higher total momentum, but for our regions of interest it is still very small. Thermal spectra are dominated by the low momentum components.

If we consider the medium rich in baryons then the difference between the polarization states becomes more important [17]. But again, for the case of interest it is negligible. The other significant argument in favor of kinetic theory is a relative simplicity of calculations enabling a transparent physical interpretation.

2.4 Differential rate calculation: mathematical formalism

For the three-particle interaction that we are dealing with here, two scenarios are possible: we either have one oncoming particle that would decay into two outgoing particles or annihilation of two oncoming particles into one outgoing. It is necessary to distinguish between these two cases.

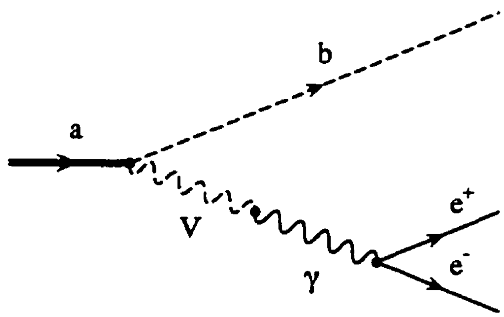

Figure 2.1: Feynman diagram of the decay $a \to b + e^+e^-$. The intermediate particle is a vector meson coupled to the photon via VMD.

First, let us consider the decay process schematically drawn in Fig. 2.1

The fundamental relativistic kinetic expression for the dilepton production rate (number of lepton pairs with invariant mass M per unit four-volume) for a process $a \to b + e^+e^-$ is

$$\frac{dR_{a\to b+e^+e^-}}{dM^2} = \mathcal{N}\int \frac{d^3p_a}{2E_a(2\pi)^3}\frac{d^3p_b}{2E_b(2\pi)^3}\frac{d^3p_+}{2E_+(2\pi)^3}\frac{d^3p_-}{2E_-(2\pi)^3}\times$$

$$\times f_a\,(1+f_b)\mid \mathcal{M}\mid^2 (2\pi)^4 \tag{2.9}$$

$$\times\delta^4(p_a-p_b-p_+-p_-)\delta(M^2-(p_++p_-)^2),$$

where f's are Bose-Einstein distribution functions, $\mathcal{N}$ is an overall degeneracy factor, and $\mid \mathcal{M}\mid^2$ is a spin-averaged squared amplitude of the process. The term $(1+f_b)$ represents the final state Bose-Einstein enhancement, an in-medium effect.

Using standard methods and spherical symmetry in momentum space this integral can be transformed to the form:

$$\frac{dR_{a\to b+e^+e^-}}{dM^2} = \frac{\mathcal{N}m_a}{(2\pi)^2}\frac{d\Gamma_{a\to b+e^+e^-}}{dM^2}\int_{m_a}^{\infty} dE_a p_a f_a(E_a) \tag{2.10}$$

$$\times\int_{-1}^{1} dx(1+f_b(E_b)),$$

with the energy of b-particle in the laboratory frame of reference E_b and in the centre of mass frame E_b^* expressed as

$$E_b = \frac{E_aE_b^* + p_ap_b^*x}{m_a} \tag{2.11}$$

$$E_b^* = \frac{m_a^2+m_b^2-M^2}{2m_a}, \tag{2.12}$$

and the differential decay width into the appropriate channel given by

$$\frac{d\Gamma_{a\to b+e^+e^-}}{dM^2} = \int \frac{1}{(2\pi)^3}\frac{1}{32m_a^3} \mid \mathcal{M} \mid^2 dt. \qquad (2.13)$$

The Lorentz-invariant Mandelstam variable t is defined in the usual way [36], $t = (p_a - p_+)^2$.

Now let us focus on the two-body channels, that is illustrated in Fig. 2.2.

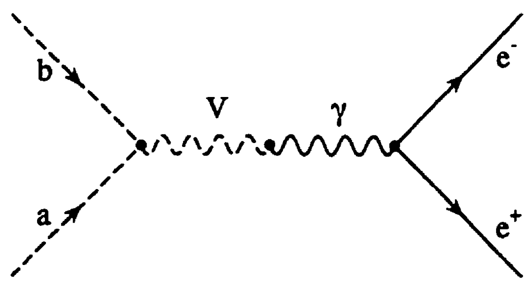

Figure 2.2: The Feynman diagram of two-body amplitude with dileptons in the final state.

The starting point in the calculations of relativistic kinetic expression for the dilepton production rate from the annihilation process $a + b \to e^+e^-$ is

$$\frac{dR_{a+b\to e^+e^-}}{dM^2} = \mathcal{N}\int \frac{d^3p_a}{2E_a(2\pi)^3}\frac{d^3p_b}{2E_b(2\pi)^3}\frac{d^3p_+}{2E_+(2\pi)^3}\frac{d^3p_-}{2E_-(2\pi)^3}$$

$$\times f_a\, f_b \mid \mathcal{M} \mid^2 (2\pi)^4 \qquad (2.14)$$

$$\times \delta^4(p_a - p_b - p_+ - p_-)\delta(M^2 - (p_+ + p_-)^2)$$

where, as in Equation 2.9, f's are the Bose-Einstein distribution functions and $\mathcal{N}$ is an overall spin-isospin degeneracy factor dependent on the specific channel.

This integral can be transformed as

$$\frac{dR_{a+b\to e^+e^-}}{dM^2} = \mathcal{N} \int \frac{d^3p_a}{(2\pi)^3}\frac{d^3p_b}{(2\pi)^3} \times f_a\, f_b\, v_{rel}\, \sigma_{a+b\to e^+e^-}\, \delta(M^2 - (p_+ + p_-)^2), \tag{2.15}$$

where the relative velocity of particles a and b is

$$v_{rel} = \frac{\sqrt{(p_a \cdot p_b)^2 - m_a^2 m_b^2}}{E_a E_b}, \tag{2.16}$$

and $\sigma_{a+b\to e^+e^-}$ is the dilepton production cross section for the process $a + b \to e^+e^-$ that is [36]

$$\sigma_{a+b\to e^+e^-} = \int \frac{d^3p_+}{2E_+(2\pi)^3}\frac{d^3p_-}{2E_-(2\pi)^3}\frac{|\mathcal{M}|^2}{4E_aE_bv_{rel}}(2\pi)^4\delta^4(p_a + p_b - p_+ - p_-). \tag{2.17}$$

Equation 2.14 can be cast into a form suitable for numerical evaluation:

$$\frac{dR_{a+b\to e^+e^-}}{dM^2} = \frac{\mathcal{N}}{32\pi^4}\int dE_a dE_b f(E_a)\, f(E_b)\lambda^{1/2}\,\sigma_{a+b\to e^+e^-}, \tag{2.18}$$

where λ is the usual kinematic triangle relation:

$$\lambda^{1/2}(M^2, m_a^2, m_b^2) = \sqrt{(M^2 - (m_a + m_b)^2)(M^2 - (m_a - m_b)^2)}. \tag{2.19}$$

We can change the meson distribution function, that we use here, from Bose-Einstein form $f_{BE}(x) = 1/(e^{x/T} - 1)$ to the Maxwell-Boltzmann one $f_{Boltz}(x) = e^{-x/T}$. This will be a poor approximation for low energies of the oncoming particles but is quite satisfactory for our range of energies. We have verified that, for the physical situation at hand, making the change implies a modification of the dilepton rate by a few percent only. The difference between the two cases (Bose-Einstein and Maxwell-Boltzmann distributions) goes to zero as the invariant mass increases. In the Maxwell-Boltzmann limit we could simplify Equation 2.18 even further [37]:

$$\frac{dR_{a+b\to e^+e^-}}{dM^2} = \mathcal{N}\frac{T}{32\pi^4 M}K_1(\frac{M}{T})\,\lambda(M^2, m_a^2, m_b^2)\,\sigma_{a+b\to e^+e^-}, \tag{2.20}$$

where K_1 is a modified Bessel function.

Throughout our work we use natural units $\hbar = c = k_B = 1$.

Chapter 3

Axial vector Lagrangians and hadronic phenomenology

The chapter is devoted to our study of axial vector ($a_1(1260)$ and $b_1(1235)$) decay contributions to the e^+e^- pair emission from the hot meson gas formed in a relativistic heavy ion collision. Using the a_1 decay study as an example a general hadronic phenomenology is introduced. Though the a_1 axial vector meson deserves attention by itself.

Recently, the role of the a_1 resonance in the photon and dilepton production from the hot hadronic matter was emphasized by several authors [25,38-41]. The reasons for such an interest towards the a_1 resonance are the following. First of all, the contribution of the a_1 in photon production has been shown to be large [25]. We want to check the validity of this result for the case of dilepton channels. Secondly, in meson environment the a_1 is an important source of lepton pairs because it is the chiral partner of ρ under $SU(2)_V \times SU(2)_A$ symmetry [42]. The importance of

ρ follows from the fact that, according to VMD, it directly couples to photon. The $\rho - a_1$ system is therefore important since it is related to spontaneous chiral symmetry breaking and restoration.

These studies are based on using various effective Lagrangians of $a_1\rho\pi$ interaction. However, different effective Lagrangians in general will give different predictions for the hadronic phenomenology that is relevant for the a_1. It is therefore necessary to know how sensitive the results are to a choice of Lagrangian. In the following we review several effective Lagrangians for $a_1\rho\pi$ vertex and calculate lepton pair production from $a_1 \to \pi\, e^+e^-$ decay by using Vector Meson Dominance (VMD) model (Equation 2.2).

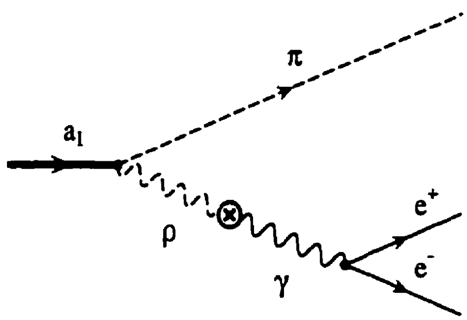

Figure 3.1: Feynman diagram for the process $a_1 \to \pi\rho \to \pi e^+e^-$

In order to come up with some feasible method of evaluation of the process we introduce two intermediate steps. As demonstrated in Figure 3.1, a_1 decays into π and ρ, ρ in its turn transforms into a photon which creates a lepton pair.

For the sake of simplicity we consider emission only of dielectrons. But the study is completely general and can be extended to include any lepton pairs.

Our choice of vector meson from the possible set of ρ, ω and ϕ mesons as of intermediate particle coupled to photon is based on isospin and G-parity arguments. We use the relativistic kinetic theory formalism for differential rate calculation we have introduced in Chapter 2.

In our survey of the $a_1\rho\pi$ interactions found in literature, we review the following effective Lagrangians:

- An effective Lagrangian used by L. Xiong, E. Shuryak and G. E. Brown [25].
- A chiral Lagrangian proposed by H. Gomm, O. Kaymakcalan and J. Schechter [40].
- A $U(2)_L \times U(2)_R$ chiral Lagrangian proposed by B. A. Li [41].

We will also introduce a new form of $b_1\omega(\phi)\pi$ effective Lagrangian and discuss its advantages in terms of the hadronic properties of the interaction. The dilepton production differential rate for the $b_1 \to \omega(\phi)\pi \to \gamma\pi \to e^+e^-\pi$ decay is also calculated.

3.1 Lagrangian used by Xiong, Shuryak, Brown

This Lagrangian was initially used in 1992 to study photon production in $\pi\rho \to \pi\gamma$ reaction through a_1 axial-vector meson [25]. For $a_1\rho\pi$ interaction it is represented in the form:

$$\mathcal{L} = G_\rho a_1^\mu (g_{\mu\nu} p \cdot q - q_\mu p_\nu) \rho^\nu \pi. \tag{3.1}$$

Here p^μ denotes the four-momentum of π and q^μ – of ρ-meson.

The coupling constant G_ρ is fitted to the strong decay width using the experimental value $\Gamma_{a_1 \to \rho\pi} = 0.4$ GeV [36]. Our result is $G_\rho = 10.5$ GeV^{-1} which is different from the original calculations [25] due to the fact that each isospin state of a_1 can undergo two possible $\rho\pi$ decays in the isospin space. This thus corrects a mistake in Ref. [25].

Since we are particularly interested in the radiative decay of a_1, we can easily construct the Lagrangian describing the process $a_1 \to \gamma\pi$ in a form

$$\mathcal{L}_{a_1\gamma\pi} = G_\gamma a_1^\mu (g_{\mu\nu} p \cdot q - q_\mu p_\nu) A_\gamma^\nu \pi. \tag{3.2}$$

According to VDM (Equation 2.2), widths of radiative and strong decays are related in such a way that:

$$\Gamma(a_1 \to \gamma\pi) = \Gamma(a_1 \to \rho\pi \to \gamma\pi) = \Gamma(a_1 \to \rho\pi) \cdot (\frac{e}{g_\rho})^2,$$

we obtain the value of the radiative coupling constant:

$$G_\gamma = G_\rho \frac{e}{g_\rho} = 0.526 \text{ GeV}^{-1},$$

which gives us the following value for the radiative decay width:

$$\Gamma_{a_1\to\gamma\pi} = \frac{G_\gamma^2|\vec{q}|}{12\pi m_{a_1}^2}(p\cdot q)^2 = 2.48\ \text{MeV}. \tag{3.3}$$

This value is somewhat larger than that measured by experiments. Yet we have to keep in mind that the experimental data for radiative decay of a_1 ($\Gamma_{a_1\to\gamma\pi} = 0.64\pm0.246$ MeV [36]) suffers from possibly large systematic errors [25]. This process is being re-measured.

The constructed Lagrangian satisfies $U(1)_{em}$ gauge symmetry. It can be easily shown. The vertex function for the Lagrangian from Equation 3.1 is

$$\Gamma^{\mu\nu} = G_\rho(g^{\mu\nu}p\cdot q - q^\mu p^\nu) \tag{3.4}$$

where μ denotes the index of a_1 and ν – of ρ-meson. Then the electromagnetic current conservation for the ρ-meson coupled to photon would imply:

$$\Gamma^{\mu\nu}\, q_\nu = G_\rho(g^{\mu\nu}p\cdot q - q^\mu p^\nu)\, q_\nu = G_\rho(q^\mu\, p\cdot q - q^\mu\, p\cdot q) = 0. \tag{3.5}$$

As a consequence, it also has to satisfy the following condition as the invariant mass of dilepton pair approaches zero. This is derived generally in Appendix A and was first suggested by L.G.Landsberg [43]:

$$\lim_{M\to 0}\frac{d\Gamma_{a_1\to\pi e^+e^-}}{dM^2} = \frac{\alpha}{3\pi M^2}\Gamma_{a_1\to\pi\gamma} \tag{3.6}$$

The above formula gives

$$\Gamma_{a_1 \to \pi\gamma} = \frac{G^2 \alpha}{24 g_\rho^2} \frac{(m_{a_1}^2 - m_\pi^2)^3}{m_{a_1}^3} \tag{3.7}$$

which is consistent with the direct calculation that led to Equation 3.3 for the strong decay width.

3.2 The Lagrangian of Gomm, Kaymakcalan, and Schechter

Now we would like to consider another effective Lagrangian for pseudoscalar, vector, and axial-vector mesons. In the original approach suggested in [40], the π meson is introduced through the nonlinear σ model, and the ρ and a_1 mesons represent massive Yang-Mills fields of the chiral symmetry. This Lagrangian has been used to describe photon and dilepton emission from hot hadronic matter [38].

We consider the vertex function for the physical $a_1 \to \pi\rho$ decay in the form [40]

$$\Gamma^{\mu\nu}_{a_1 \to \pi\rho} = i(j\, g^{\mu\nu} - h\, q^\mu k^\nu), \tag{3.8}$$

where there are two momentum-dependent constants

$$j = \frac{g}{\sqrt{2}}[-\eta_1 q^2 + (\eta_1 - \eta_2)k \cdot q],$$

$$h = \frac{g}{\sqrt{2}}(\eta_1 - \eta_2),$$

with

$$\eta_1 = (\frac{1-\sigma}{1+\sigma})^{1/2}(\frac{gF_\pi}{2m_\rho^2}) + \frac{4\xi Z^2}{F_\pi\sqrt{1+\sigma}},$$

$$\eta_2 = (\frac{1+\sigma}{1-\sigma})^{1/2}(\frac{gF_\pi}{2m_\rho^2}) - \frac{4\sigma}{gF_\pi\sqrt{1-\sigma^2}}$$

and

$$Z^2 = 1 - \frac{g^2F_\pi^2}{4m_\rho^2}.$$

Here $F_\pi = 135$ MeV is the pion decay constant.

We derive two sets (see Table 3.1) of parameters fitted to the experimentally measured strong decay width $\Gamma_{a_1 \to \rho\pi} = 0.4$ GeV [36]. The ratio of D-wave and S-wave (eigenstates of the relative orbital angular momentum in the exit channel) amplitudes can be calculated and is presented in detail in Appendix B.

We have considered both parameterizations although parameter set 2 fits the D/S ratio, $D/S = -0.09 \pm 0.03$, that has been measured experimentally [36], much better

	g	σ	ξ	D/S
GKS1	10.3	0.341	0.447	0.357
GKS2	6.448	-0.291	0.059	-0.099

Table 3.1: Parameter sets and D/S ratio for Gomm, Kaymakcalan, Schechter Lagrangian.

than parameter set 1. Calculated radiative decay widths for sets 1 and 2 are $\Gamma^{(1)}_{a_1 \to \pi\gamma} = 4.5$ MeV and $\Gamma^{(2)}_{a_1 \to \pi\gamma} = 0.067$ MeV respectively.

The electromagnetic interaction is introduced by imposing electromagnetic gauge invariance. Ward identity can be shown to hold in the same way as in Equation 3.5 with the corresponding vertex function from Equation 3.8. As a consequence, Formula 3.6 is valid as well.

3.3 $U(2)_L \times U(2)_R$ chiral Lagrangian of Li

This study of $U(2)_L \times U(2)_R$ chiral theory of pseudoscalar, vector and axial-vector mesons has been proposed by Bing An Li [41] in 1995. The $a_1(k)\pi(p)\rho(q)$ coupling is described by the following effective chiral Lagrangian:

$$\mathcal{L} = A\, \vec{a}_\mu \cdot (\vec{\rho}_\mu \times \vec{\pi}) + B\, \vec{a}_\mu \cdot (\vec{\rho}^\nu \times \partial_{\mu\nu} \vec{\pi}), \qquad (3.9)$$

where again A and B are momentum-dependent coefficients

$$A = \frac{2}{f_\pi}\sqrt{(1-\frac{1}{2\pi^2 g^2})\frac{F^2}{g^2}+\frac{m_a^2}{2\pi^2 g^2}}$$

$$-\frac{2c}{g}(p\cdot q + p\cdot k) - \frac{3}{2\pi^2 g^2}(1-\frac{2c}{g})p\cdot q,$$

$$B = -\frac{2}{f_\pi}\sqrt{(1-\frac{1}{2\pi^2 g^2})\frac{1}{2\pi^2 g^2}(1-\frac{1}{2\pi^2 g^2})},$$

and c, F^2 and g are input parameters:

$$c = \frac{f_\pi^2}{2gm_\rho^2}, \qquad F^2 = \frac{f_\pi^2}{1-\frac{2c}{g}}.$$

The particle masses are taken as input. We fix $f_\pi = 0.186$ GeV and $g = 0.35$ as suggested in [41].

In order to satisfy the current conservation in the case of a real photon we have to impose the following constraint on the interaction Lagrangian:

$$A(q^2=0) = \frac{1}{2}(m_{a_1}^2 - m_\pi^2)B. \tag{3.10}$$

In the original paper [41] the mass of π-meson is set to be zero. For the consistency of our approach we kept the mass of π-meson finite throughout all of our calculations. As it is shown in Figure 3.2, only in the region of high invariant mass of the dilepton

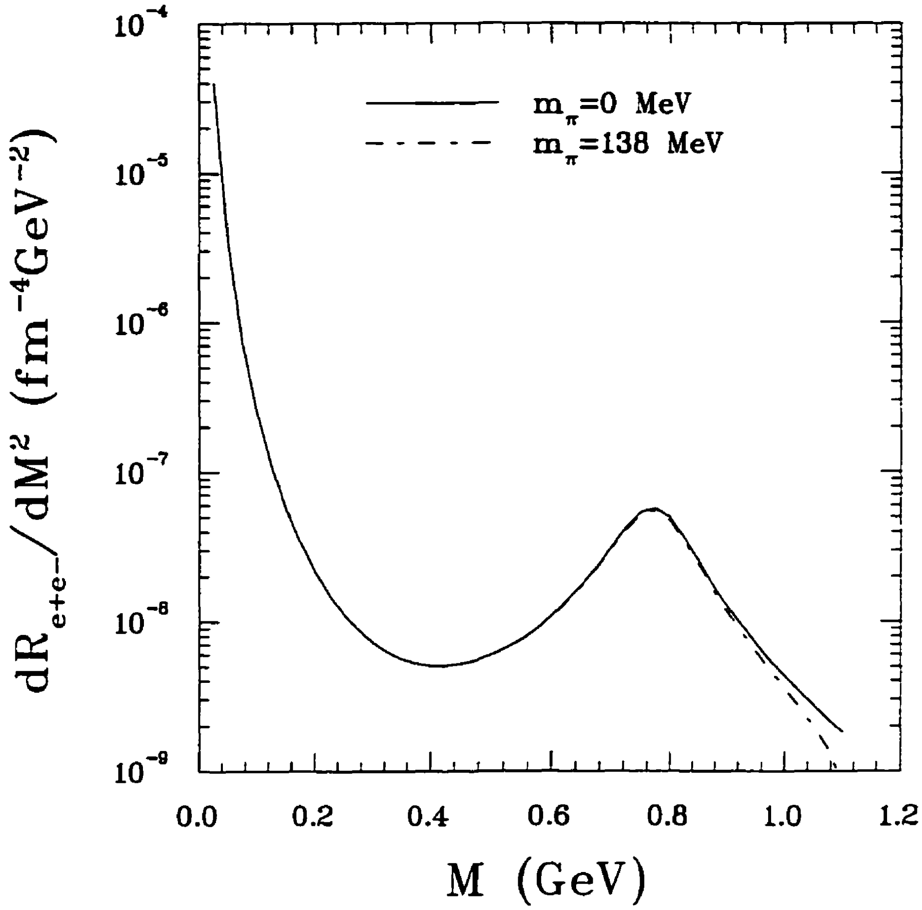

Figure 3.2: Dielectron production rate calculated using Li Lagrangian with and without taking into account finite mass of π-meson at $T = 150$ MeV.

pair there is only a slight difference in the final results for dilepton emission rate depending on whether m_π is zero or finite.

Using suggested set of constants we find the value of the radiative decay width to be 278 keV and the strong decay width to be 258 MeV.

3.4 Comparison

In this section we will compare rates of the lepton pair emission calculated using effective Lagrangians introduced earlier.

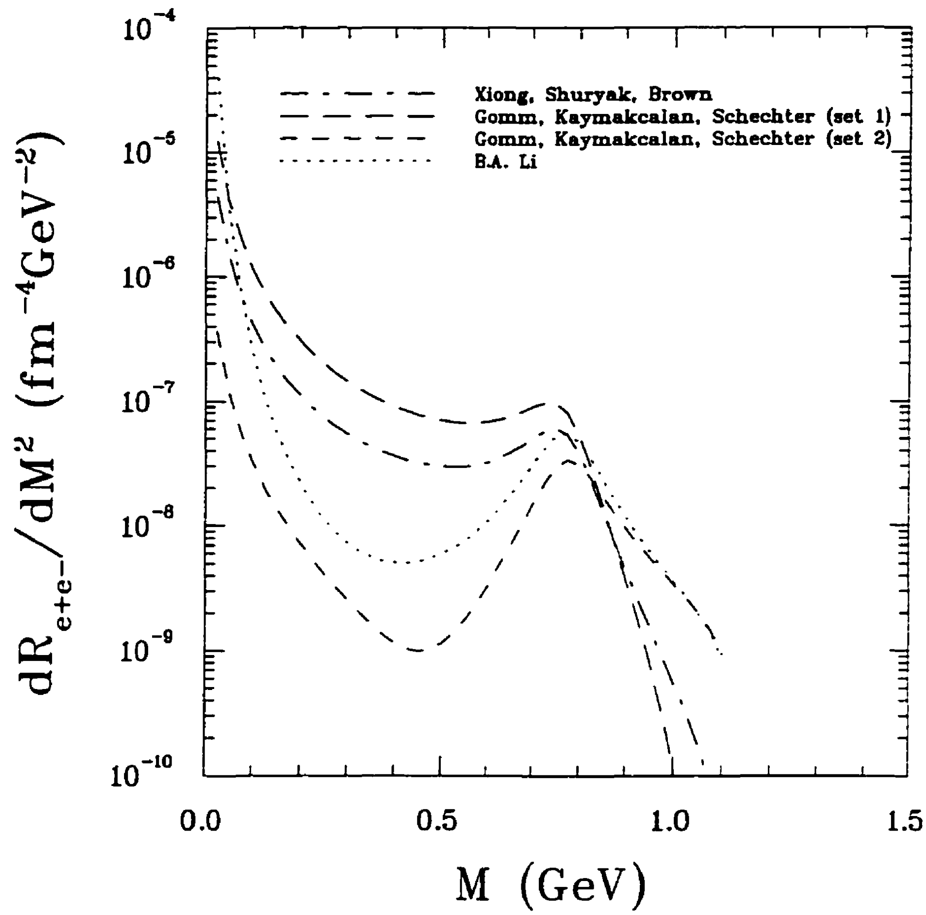

Figure 3.3: Dielectron production rates versus invariant mass of lepton pair calculated using different interaction Lagrangians at T =150 MeV.

In Figure 3.3 dielectron production rates for the a_1 decay, calculated using different effective Lagrangians, are plotted. As it can be seen, the contributions are quite different. In order to judge the quality of our results and to comment on the restrictions imposed on the effective interactions by the hadronic properties, let us first compare them to each other and, secondly, to empirical measurements.

Source:	XSB	GKS1	GKS2	Li	Data
$\Gamma_{a_1\pi\rho}$	fit	fit	fit	258	400
$\Gamma_{a_1\pi\gamma}$	2.48	4.5	0.067	0.278	0.64±0.25
D/S	0.185	0.357	-0.099	-0.161	-0.09±0.03
χ^2	37.3	156.	1.8	3.1	

Table 3.2: Comparison of hadronic properties for the discussed interaction Lagrangians (width is in MeV).

In Table 3.2 we display the calculated strong and radiative widths and D/S ratios for the discussed interaction Lagrangians and compare them with experimental measurements.

Using χ^2 as a goodness-of-fit criterion, we could classify the $a_1\pi\rho$ interaction Lagrangians going from the "worst" to the "best" reproduction of the experimental data:

$$\text{GKS1} \longrightarrow \text{XSB} \longrightarrow \text{Li} \longrightarrow \text{GKS2}$$

How does our conclusion reflect the choice of the best plot in the graph? Looking at

Figure 3.3 one can deduce that the differential rates get smaller as they fit better.

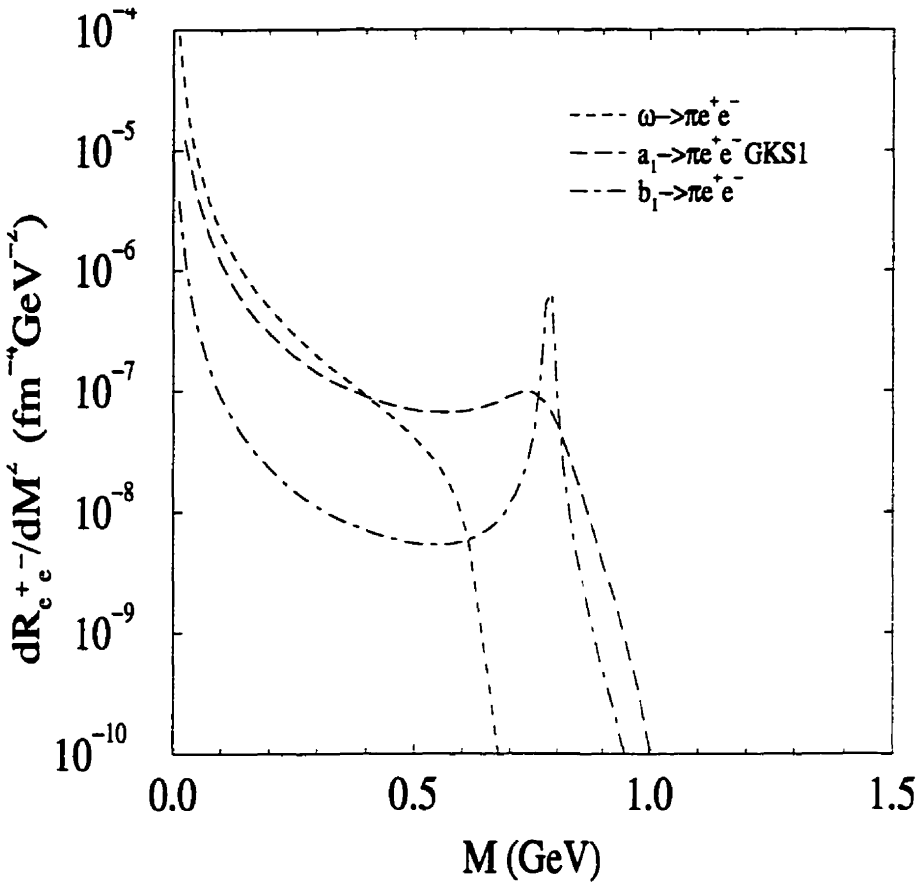

Figure 3.4: Dielectron production rates of the b_1, ω decays and a_1 decay calculated using Gomm, Kaymakcalan, Schechter Lagrangian (parameter set 1) at T =150 MeV.

The divergence among the differential rates in Figure 3.3 at the photon point (M=0) can be attributed to the fact that the coupling constants are fitted to the strong decay data for most of the considered Lagrangians (see Table 3.2). Radiative decay width remains unaccounted for. If one fits the strength of interaction to the radiative decay data all the rates at the photon point come to the same value. The exception is the Lagrangian by Li where the choice of the constants is based on different arguments (see Page 27).

To conclude, let us look one more time at the graph for lepton pair production differential rates and think if our statement about best fitting Lagrangian can be verified experimentally. Unfortunately, currently for the hot meson environment in heavy ion collisions it is hard to isolate experimental data on a_1 decay since there is a channel that will outshine even our worst hadronic fit (the highest one on the plot) in the region of invariant mass $M < 0.5$ MeV where the difference between chosen Lagrangians is especially significant. It is illustrated Figure 3.4. This channel is $\omega \rightarrow \pi\, e^+e^-$. Further research (see Page 33) shows that for the region of invariant mass of lepton pair around ρ/ω meson rest mass, the contribution that outshines both channels (a_1 and ω) comes from the decaying b_1. But this peaks in a very narrow region of invariant mass.

3.5 Effective Lagrangian for $b_1\omega(\phi)\pi$ interaction

It would be of particular interest to compare the contributions of the two lightest well-established axial vector mesons to lepton pair production. For the $b_1 \rightarrow e^+e^-\pi$ decay we follow the sequence of intermediate steps $b_1 \rightarrow \omega(\phi)\pi \rightarrow \gamma\pi \rightarrow e^+e^-\pi$ in a complete agreement with the scenario suggested for the a_1 decay. Our choice of VMD intermediate particle coupled to the photon is based on the isospin and G-parity arguments which in this particular case lead us to ω and ϕ vector mesons.

The strong interaction Lagrangian for the vertex $b_1\omega(\phi)\pi$ is proposed to be:

$$\mathcal{L}_{b_1\pi\omega(\phi)} = g_{b_1}\vec{\pi}\cdot\vec{b}_1^{\mu\nu}\left(\frac{\omega^8_{\mu\nu}+\sqrt{2}\omega^s_{\mu\nu}}{\sqrt{3}}\right) + h_{b_1}\partial^\nu\vec{\pi}\cdot\vec{b}_1^\mu\left(\frac{\omega^8_{\mu\nu}+\sqrt{2}\omega^s_{\mu\nu}}{\sqrt{3}}\right) \tag{3.11}$$

where notation field$^{\mu\nu}$ stands for (∂^μfield$^\nu - \partial^\nu$field$^\mu$) and the octet and singlet fields, ω^8 and ω^s, are expressed in terms of the physical fields with a mixing angle θ_V:

$$\omega^8 = \phi\cos\theta_V + \omega\sin\theta_V,$$

$$\omega^s = \omega\cos\theta_V - \phi\sin\theta_V$$

The mixing angle is fitted to reproduce radiative decay phenomenology [44].

Our choice of this particular Lagrangian (different from the Lagrangian first suggested in [33]) for $b_1\pi\omega(\phi)$ interaction is based on the requirement of the electromagnetic current conservation which was not satisfied for the Lagrangian from [33]. This requirement is a necessary restriction since in the present work we consider the radiative rather than strong decay of b_1. It is easy to show that our Lagrangian from Equation 3.11 satisfies $U(1)_{em}$ gauge symmetry without any additional restrictions on the form of interaction. The existence of two independent coupling constants g_{b_1} and h_{b_1} leaves us freedom in reproducing the hadronic properties of b_1. They are inferred to fit the strong decay width and the ratio of the D wave content of the decay amplitude to its S wave content. The prescription for D/S ratio calculation is analogous to the one presented in Appendix B for the case of $a_1 \rightarrow \rho\pi$ decay. Analysis of the experimental data gives us $g_{b_1} = -1.065$ GeV^{-1} and $h_{b_1} = 15.13$ GeV^{-1}.

The reaction $b_1 \rightarrow e^+e^-\pi$ is possible via either ω or ϕ. But here we invoke [36] that b_1 has a branching ratio of more than 50% into $\omega\pi$ and less than 1.5% into $\phi\pi$.

Consequently, we consider the intermediate ϕ contribution to be negligible compared to ω being an intermediate particle coupled to virtual photon.

The dilepton production differential rate of b_1 decay is presented in Figure 3.4 along with the contributions from a_1 and ω channels. One can see that in the very narrow region of invariant mass of lepton pair around ρ/ω rest mass b_1 is a leading contribution among those three decays. In a later chapter (see Page 45) we will see that both axial vector meson decay contributions still can be considered small compared to the contributions of some of the constituents of the meson bath created in the heavy ion collision.

3.6 Summary

In order to come up with some quantitative description of the lepton pair production due to the axial vector decays in the hot meson gas produced in the course of ultra-relativistic heavy ion collision, we have considered different effective Lagrangians for the $a_1\rho\pi$ interaction and a new effective Lagrangian for the b_1 strong decay. The a_1 decay contribution previously was not surveyed using such sophisticated Lagrangians as considered here. Some restrictions imposed on the effective interactions by the hadronic properties justified the choice of the best Lagrangian. The analysis has led us to the following conclusions:

- Dilepton production differential rates differ significantly depending on the type of strong interaction Lagrangian that is used.

- Special care must be taken respecting type of the interaction Lagrangian. Our choice must be based on comparison with the experimentally measured hadronic properties.

- Among known $a_1 \rightarrow \pi\, e^+e^-$ Lagrangians, Gomm, Kaymakcalan, Schechter Lagrangian (parameter set 2) fits experimental data better.

- Presently, it is difficult to get experimental evidence in heavy ion collisions to support our judgment of how "good" the a_1 Lagrangian is. In the hot meson environment created in relativistic heavy ion collisions there are processes that yield greater contributions.

- In the region of low invariant mass of lepton pair (LMR) the contribution from the decay of ω meson will outshine the a_1 contribution. Around the ρ/ω meson rest mass the b_1 axial vector decay was found to outshine both of the above mentioned channels (a_1 and ω). Despite that, both axial vector meson decay contributions to the dilepton production remain small compared to the decay of some of the constituents of the meson bath created in the heavy ion collision.

- We therefore conclude that the detection of an electromagnetic signature of the axial mesons still constitutes a challenge in the LMR. We will confirm this last statement quantitatively in the next chapter.

Chapter 4

Low and intermediate mass dileptons from a hot bath of light mesons

In this chapter we present our results of a systematic study of the meson medium contribution to the dilepton emission from the hot fireball formed in ultrarelativistic nuclear collisions. Using relativistic kinetic theory formalism, the low and intermediate mass dilepton production rate ($M < 3$ GeV) is calculated. Special attention is paid to experimental data on the time-reversed processes in order to constrain an "effective form factor" of the reactions. The most significantly contributing decays and reactions among all allowed by the conservation laws are considered. In order to prove that our analysis includes all the important channels, a comparison of the obtained total dilepton rate with the recent data obtained using the collection of spectral functions which are extracted from e^+e^- annihilation and τ lepton decay data in the low and intermediate mass region [26] is carried out.

4.1 Introduction

Previous calculations of dilepton emission rate [30] were carried out for a variety of reactions and decays in a hot meson environment. For the sake of completeness, we expand a list of the entrance channels. To our knowledge ours is the most complete list of various mesonic contributions to the dilepton production in heavy ion collisions that include axial vectors.

We have chosen a temperature of T=150 MeV in accordance with the arguments presented on Page 2 and simply to fix ideas.

The hot hadronic bath is assumed to be a collection of light strange and nonstrange mesons. We consider interaction among mesons up to the lowest nonvanishing order, which according to the argument presented on Page 9 is three particles strong interaction. It would introduce two possible types of mesonic reactions leading to lepton pair emission:

$$a \to b\ e^+e^- \qquad \text{and} \qquad a + b \to e^+e^-.$$

P	V	A
π, K, η, η'	ρ, ω, ϕ, K^*	a_1, b_1

Table 4.1: List of all considered light mesons

We want to check if the size of our total considered contribution is consistent with some of the previously calculated results. The appropriate information at hand [26] provides us with the data on the low as well as on the intermediate invariant mass region. That is why we have to include into our consideration the region of the low invariant mass though it is not of any particular interest with respect to the main goal of our research: signature of QGP. That is the reason why special attention is paid in this chapter to the decay processes. We also want to confirm quantitatively the unfortunate finding of the previous chapter: there is no electromagnetic signal of the axial mesons in the low mass sector.

We include all possible interaction channels that are not forbidden by conservation laws. In Table 4.1 we list all mesons of interest classified into three main groups: pseudoscalar, vector, and axial-vector mesons.

Depending on the combination of participating mesons we choose the corresponding interaction Lagrangian. It can be PPV, VVP, VVV, or PVA Lagrangian from Equations 2.5,2.6, 2.8, and 3.8, respectively.

4.2 Decay processes contributing to e^+e^- emission

Let us now consider decay processes $a \to b\ e^+e^-$ in a hot meson bath that contribute to the lepton pair production.

The first restriction comes from the fact that secondary b particle is at least as heavy as a light pseudoscalar meson. Hence, all the processes with a light pseudoscalar as a decaying particle are immediately ruled out because of energy conservation. For η' decay, the corresponding radiative decay width is far too small ($\Gamma(\eta' \to \rho^0\gamma) = 90$ keV) to give any significant contribution. So we neglect this channel. Strange mesons $K^{0,\pm}$ were not observed in radiative decays at all. As for K^*, their radiative decay widths are very small [36]. Therefore, the strange meson decays can be omitted from our consideration. At the end of the day we are left with ρ, ω, ϕ, b_1, and a_1 decays.

In Table 4.2 all the possible decay channels that have, according to [36], nonvanishing decay widths are listed. Our choice of the intermediate vector particles is based on G-parity and isospin conservation at the strong vertex.

We neglect the last two decays of ϕ meson as not contributing significantly because the respective coupling constants are much too small. Besides, these channels would contribute just to the region of the invariant mass smaller than $m_\phi - m_\omega = 0.238$ GeV for the first channel and $m_\phi - m_\rho = 0.25$ GeV for the second one and are not of particular interest.

The interaction Lagrangian from Equation 2.6 is employed for the calculation of ρ, ω and ϕ decay amplitudes. The ratio of coupling constants $G_{VVP}/g_{\rho(\omega,\phi)}$ is adjusted so that the experimentally measured radiative decay widths would be reproduced. Via this procedure one can fix only the ratio of strong to electromagnetic (vector meson to photon) coupling. However, this is exactly the combination we need in order to calculate the dilepton production. A particular example of such calculations for the case of a_1 decay is considered on Page 22.

For the decay $\phi \to \pi\rho \to \pi\gamma^* \to \pi e^+e^-$ it is possible to fit the required coupling

ρ	$\rho \to \pi\gamma^* \to \pi e^+e^-$ $\rho^0 \to \eta\gamma^* \to \eta e^+e^-$	$\Gamma_{\pi\gamma}/\Gamma_{tot} = 4.5 \cdot 10^{-4}$ $\Gamma_{\eta\gamma}/\Gamma_{tot} = 3.8 \cdot 10^{-4}$
ω	$\omega \to \pi^0\gamma^* \to \pi^0 e^+e^-$ $\omega \to \eta\gamma^* \to \eta e^+e^-$	$\Gamma_{\pi^0\gamma}/\Gamma_{tot} = 8.5\%$ $\Gamma_{\eta\gamma}/\Gamma_{tot} = 8.3 \cdot 10^{-4}$
ϕ	$\phi \to \pi\rho \to \pi\gamma^* \to \pi e^+e^-$ $\phi \to \eta\gamma^* \to \eta e^+e^-$ $\phi \to \omega\gamma^* \to \omega e^+e^-$ $\phi \to \rho\gamma^* \to \rho e^+e^-$	$\Gamma_{\pi\rho}/\Gamma_{tot} = 12.9\%$ $\Gamma_{\eta\gamma}/\Gamma_{tot} = 1.26\%$ $\Gamma_{\omega\gamma}/\Gamma_{tot} < 5\%$ $\Gamma_{\rho\gamma}/\Gamma_{tot} < 2\%$
b_1	$b_1 \to \pi\omega \to \pi\gamma^* \to \pi e^+e^-$	$\Gamma_{\pi\omega} = 0.142$ GeV
a_1	$a_1 \to \pi\rho \to \pi\gamma^* \to \pi e^+e^-$	$\Gamma_{\pi\omega} = 0.4$ GeV

Table 4.2: List of all existing decay channels included in this work that can produce a lepton pair.

constant G_{VVP} to the data on strong decay width and relate it later to the known [27] VMD coupling constant $g_\rho = 6.06$ to obtain the desired ratio G_{VVP}/g_ρ.

For the b_1 decay (PVA strong interaction) we used the interaction Lagrangian from Equation 3.11 with the coupling constants inferred to fit the strong decay width and the ratio of the D wave content of the decay amplitude to its S wave content. Analysis of the experimental data gave us $g_{b_1} = -1.065\ \mathrm{GeV}^{-1}$ and $h_{b_1} = 15.13\ \mathrm{GeV}^{-1}$.

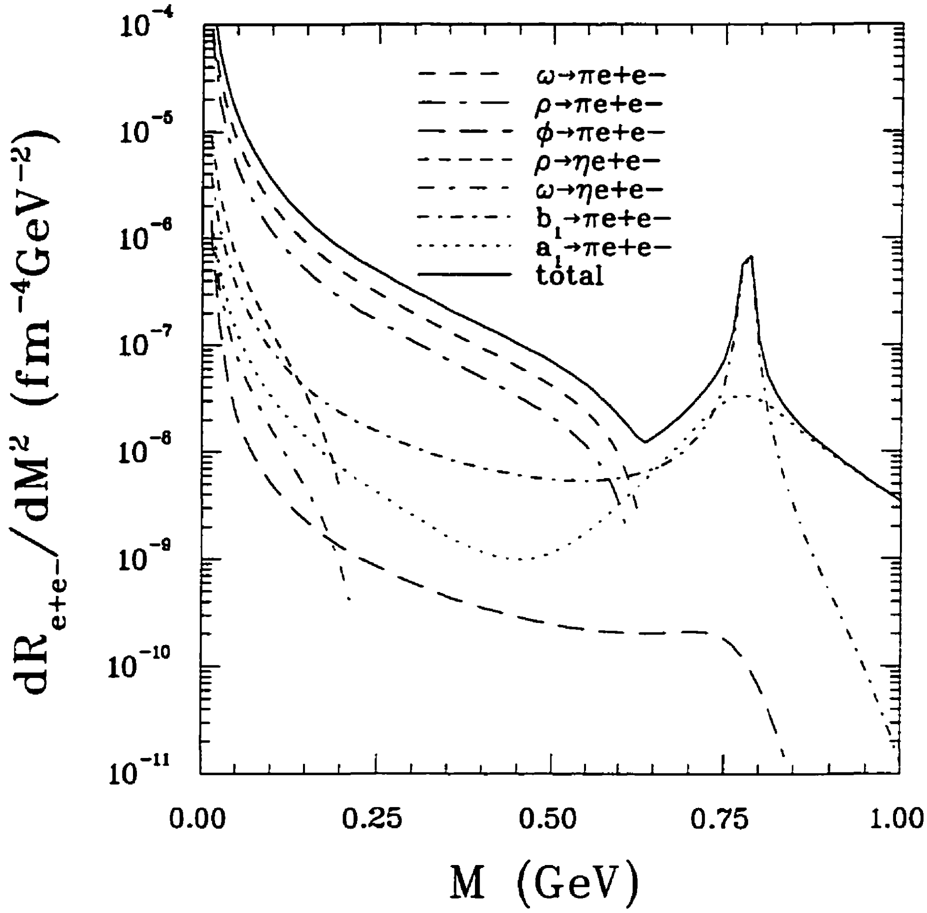

Figure 4.1: Differential rate of lepton pair production via light mesons decay at a temperature $T = 150$ MeV. The solid line is the sum of all the decay processes listed in the legend of the plot.

In the case of a_1 decay (PVA strong vertex) we employ the interaction Lagrangian from Equation 3.8 with the parameter set 2 (see Table 3.1) that is shown to reproduce the hadronic properties of a_1 resonance better than the other effective Lagrangians. Chapter 3 is devoted to the discussion on the choice of the interaction Lagrangian for the lepton pair production through a_1 decay.

In the dilepton production rate calculation we follow the procedure introduced in Section 2.4. First of all, the square of the spin-averaged amplitude of the process is calculated. Due to the complexity of this procedure we have used "Mathematica". Then we use the Equation 2.13 to obtain the differential width of the appropriate channel. Finally, the width is substituted into Equation 2.10 giving us the differential rate of lepton pair production.

The results at a temperature $T = 150$ MeV are shown in Figure 4.1. For soft dileptons the dominant contribution comes from the ω decay. For considered interval of invariant mass, the $\rho \to \pi e^+e^-$ decay represents the next-to-leading contribution. Contributions of other channels are at least an order of magnitude smaller. For the narrow region of invariant mass of lepton pair around ρ/ω meson rest mass, the dominant contribution comes from the decaying b_1. This happens because in this region the ω, one of two intermediate particles in the b_1 decay, has a narrower peak (a smaller width) than the ρ meson, which is a mediator in the a_1 decay. The a_1 channel plays more important role as the invariant mass of dileptons exceeds 0.8 GeV. Unfortunately even after our analysis, we can not prove that the axial vectors can shine through the other mesons. We will therefore not consider the low mass region any longer.

4.3 Two-body meson reactions as a source of lepton pairs

After initial stages of a collision, which may include a prehadronic and QGP phase, hadronization gives rise to a hot mixture of the lighter mesons: pions and resonances (ρ,ω-mesons, etc.) which interact with each other [23]. In the light of the general idea of collective phenomena in the dense and hot fireball, created in ultra-relativistic heavy ion collisions, special attention must be paid to the reactions between those constituents as possibly contributing to the dilepton production. Let us follow the same ideology as in Section 4.2. In order to determine what channels should be included into consideration let us recall that for strong vertex the outgoing particle must be the VMD vector meson, namely, ρ,ω or ϕ. Since we take into account only three point vertices, the strong interaction must be one of the following: P+P $\rightarrow$ V, V+V $\rightarrow$ V, V+P $\rightarrow$ V, or A+P $\rightarrow$ V with participating particles from Table 4.1.

The mathematical procedure of the dilepton production differential rate calculation is described in Section 2.4. We use Equation 2.20 for the rate and Equation 2.17 for the cross section calculations.

Since the phase space now allows a collection of intermediate-mass vector mesons to be accessed, the experimental form factors containing intermediate vector particles become important here. Whenever there are available experimental data on the corresponding time-reversed process we employ them in order to constrain an effective form factor of the reaction. The ρ and ϕ vector mesons have been given the same form factors as their corresponding pseudoscalar counterparts from e^+e^- annihilation channels. It means that whenever we had to use the intermediate vector meson form factor , we used instead the experimental information available on electromagnetic form factor of pions (for ρ meson) [45] and kaons (for ϕ meson) [46]. The recent parameterization of experimental data from [47] was employed. For the ω meson propagation we used a simple one-pole parameterization. Since we fix the coupling constants by fitting them to the radiative decay width, the suggested method can be treated analogously to introducing the invariant mass dependent coupling constant.

Among all the combinations of two incoming pseudoscalar and one outgoing vector mesons from Table 4.1, only the following have non-vanishing experimental coupling constants:

$$\pi + \bar{\pi} \rightarrow \rho \rightarrow e^+e^-,$$

$$K + \bar{K} \rightarrow \phi \rightarrow e^+e^-,$$

$$\eta + \pi^0 \rightarrow \omega \rightarrow e^+e^-.$$

The way we determine the strength of the strong interaction $a + b \rightarrow V$ is based on the experimental estimation of the VMD meson strong decay $V \rightarrow a + b$ interaction strength. The coupling constants of both reactions are assumed to be invariant with respect to the direction of the reaction. Consequently, the last channel has a very small coupling constant, since the experimentally determined width of the inverse reaction $\omega \rightarrow \eta + \pi^0$, is small compared to the first two channels ($\Gamma_{\omega \rightarrow \eta + \pi^0} = 8.43 \times 10^{-6}$ GeV with Confidence Level CL=90 %). Hence, it does not contribute significantly to the dilepton rate. The interaction Lagrangian for the first two channels is presented by Equation 2.5.

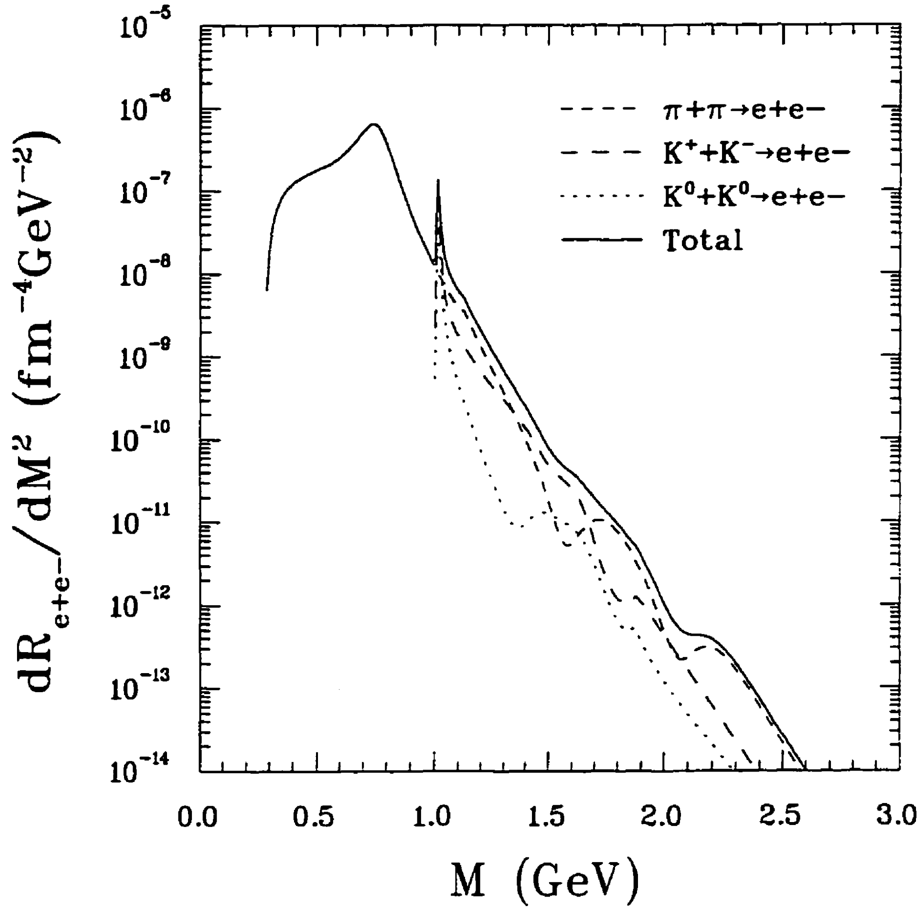

Figure 4.2: Lepton pair differential rate from P+P reaction type at a temperature $T = 150$ MeV. The solid line is the sum of all P+P processes listed in the legend of the plot.

We show the results for P+P $\to e^+e^-$ in Figure 4.2. It can be seen that the only apparent structures in the resulting curve are due to the $\rho(770)$ and ϕ peaks with a slight rise corresponding to $\rho(2150)$. All other bumps in a particular channel reflect the structure of the effective form factor of an intermediate vector meson inferred from experimental data on e^+e^- annihilation.

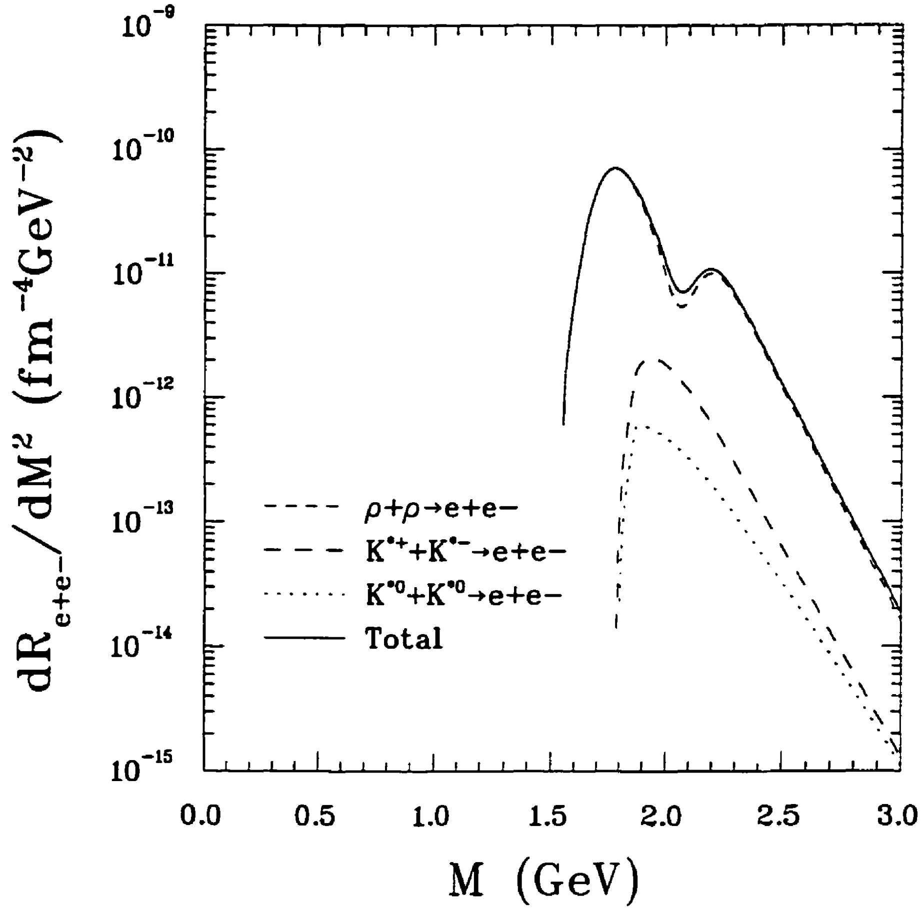

Figure 4.3: Lepton pair differential rate from V+V reaction type at a temperature $T = 150$ MeV. The solid line is the sum of all V+V processes listed in the legend of the plot.

Let us consider now V+V reaction channels. There will be just two allowed processes contributing to the e^+e^- emission:

$$\rho^+ + \rho^- \to \rho^0 \to e^+e^-,$$

$$K^* + \bar{K}^* \rightarrow \phi \rightarrow e^+e^-$$

Once again we use experimentally-fitted form factors of the ρ and ϕ mesons. The results are shown in Figure 4.3. For the $\rho^+ + \rho^-$ channel two peaks correspond to the excitations of ρ: at $M = 1690$ MeV and at $M = 2150$ MeV. It is clear that the strange mesons K^* do not contribute significantly to the resulting curve of the dilepton production rate for the V+V reaction channels.

For a pseudoscalar interacting with a vector meson the allowed processes are:

$$\omega + \pi^0 \rightarrow \rho \rightarrow e^+e^-,$$

$$\rho + \pi \rightarrow \omega/\phi \rightarrow e^+e^-,$$

$$\rho^0 + \eta \rightarrow \rho \rightarrow e^+e^-,$$

$$\phi + \pi^0 \rightarrow \rho \rightarrow e^+e^-,$$

$$K + \bar{K}^* \rightarrow \phi \rightarrow e^+e^-.$$

For the second process in the list, G-parity arguments allow either ω or ϕ meson to be an intermediate VDM particle. Since the threshold of the reaction lies just below the ϕ-peak, it is important to account for both of them. We apply a two-poles formula for the form factor by introducing the mixing angle between ω and ϕ [48].

The fourth reaction has a very small coupling constant due to the fact that $\Gamma_{\rho \rightarrow \phi + \pi^0} <$ 1.0 MeV and we do not include it in our consideration. As for the last channel its contribution is roughly of the size of the one from $\pi + \rho$ [30].

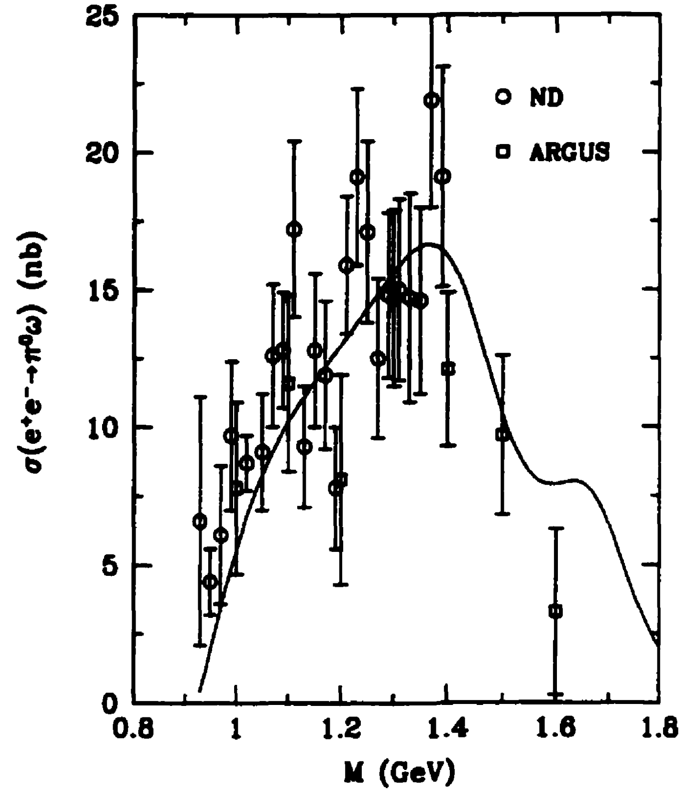

Figure 4.4: The cross section for $e^+e^- \to \pi^0\omega$. The solid curve is based on the model of Ref. [49]. The experimental data are from the ND Collaboration [49](circles) and the ARGUS Collaboration [50](squares).

The differential rate calculations in the case of $\omega + \pi$ reaction are based on the fit to the experimental cross section data for $e^+e^- \to \pi^0\omega$ from the ND Collaboration [49] and the ARGUS Collaboration [50] which is shown on Figure 4.4. The simple one-pole $\rho(770\,\text{MeV})$ form factor gives us the rate clearly smaller than the one calculated using the experimental cross section.

For the A+P $\rightarrow$ V type of interaction the main channels are

$$a_1 + \pi \rightarrow \rho \rightarrow e^+e^-,$$

$$b_1 + \pi \rightarrow \omega/\phi \rightarrow e^+e^-.$$

There are experimental data on the process $e^+e^- \rightarrow a_1 + \pi$ determined by DM2 Collaboration by partial wave analysis [51]. We show them in Figure 4.5. The fit to the experimental cross section of such a reaction is employed in order to estimate the intermediate-mass form factor. In Chapter 3 we discussed a choice of an effective Lagrangian for $a_1\pi\rho$ strong interaction that better reproduces the experimental hadronic properties. Now, calculating the amplitude of the process, we use the most promising one.

For $b_1\pi\omega(\phi)$ interaction the effective Lagrangian corresponds to Equation 3.11. This channel is possible via either ω or ϕ. But here we have to remember [36] that b_1 has a branching ratio of more than 50% into $\omega\pi$ and less than 1.5% into $\phi\pi$. Consequently, we consider the intermediate ϕ contribution to be negligible compared to ω as an intermediate particle coupled to virtual photon.

The results for V+P and A+P reactions for the temperature 150 MeV are shown in Figure 4.6. The most significant contribution for the considered here mass region is coming from $\omega + \pi$ channel. It is not surprising, since the decay width of inverse reaction $\rho(1690) \rightarrow \omega + \pi$ is quite large ($\Gamma_{\rho\rightarrow\omega+\pi} = 30.4$ MeV) compared, for example, to $\phi \rightarrow \rho + \pi$ ($\Gamma_{\phi\rightarrow\rho+\pi} = 0.57$ MeV).

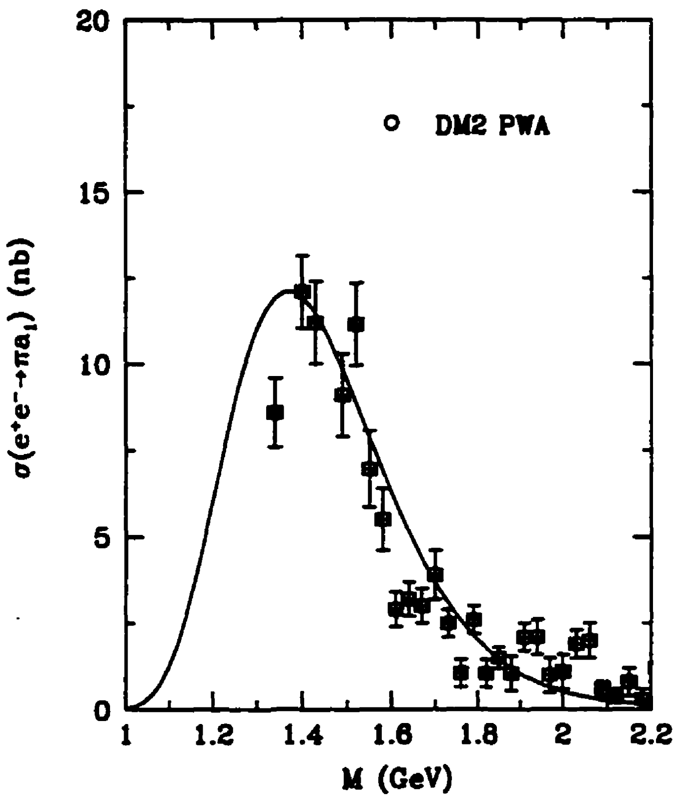

Figure 4.5: The cross section for $e^+e^- \to \pi a_1$. The open circles are the experimental data determined by the DM2 Collaboration using partial wave analysis [51]. The solid curve represents the fit used in our calculations.

Finally, the total rate of all discussed processes is plotted in Figure 4.7 along with the recent data obtained using a collection of spectral functions which are extracted from e^+e^- annihilation and τ lepton decay [26]. These data claim to reflect the phenomenological properties of the lepton pair emission because it uses the most general form of the spectral functions and, hence, accounts for all axial-vectors, vectors, and

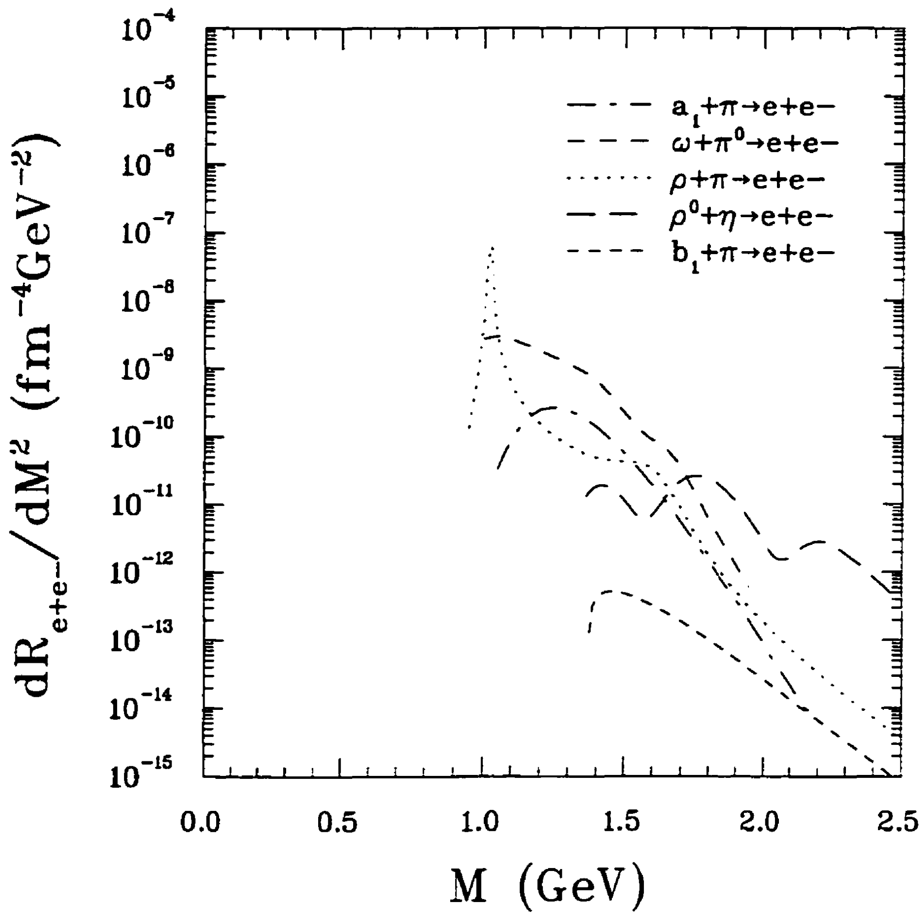

Figure 4.6: Lepton pair differential rate from V+P and A+P reaction types at a temperature $T = 150$ MeV.

pseudoscalars mesonic contributions. It can be seen that our predictions coincide with the above mentioned points quite nicely. The divergence of experimental data from our theoretical curve in the region of invariant mass $\sim M = 400$ MeV can be attributed to the neglect of radiative decay contributions in the analysis of [26].

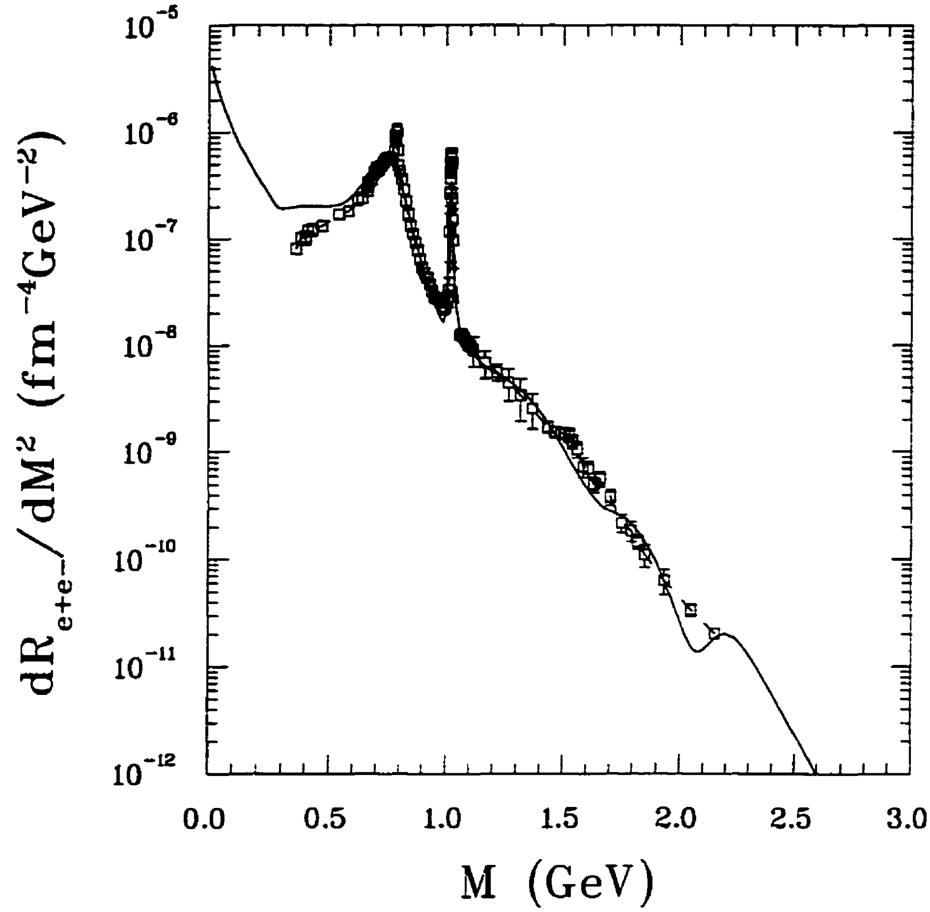

Figure 4.7: Total lepton pair production rate from hot meson bath at a temperature $T = 150$ MeV. The data are from [26].

4.4 Summary

A systematic research on the light meson contribution to the dilepton emission in ultra-relativistic heavy ion collisions has been performed. The most contributing decays and reactions among all allowed by the conservation laws are calculated and summed for the low (LMR) and intermediate (IMR) dilepton mass (up to $M = 3$ GeV) production rate.

In order to justify that our analysis accounts for all the important channels we compare the total dilepton rate with the data obtained using the collection of spectral functions extracted from e^+e^- annihilation and τ lepton decay by Z.Huang [26]. His analysis was concerned with summing up the largest possible amount of channels that will produce dileptons. As the result of the comparison we claim that our analysis does include all the important channels in the low and intermediate mass region.

In the region of invariant mass below the ρ-meson rest mass the ω-meson decay is a dominant contribution. At invariant mass above 1.0 GeV, the contribution from light meson decays sharply drops off due to their insufficient mass, and the associated two-body reactions give rise to the dilepton production.

In the next Chapter, we apply the obtained results to the calculation of lepton pair production rate using hydrodynamic model of heavy ion collisions.

Chapter 5

Application to intermediate mass dilepton production in relativistic heavy ion collisions

One of the main goals of ultra-relativistic heavy-ion physics is the creation of a quark-gluon plasma (QGP). This Chapter addresses the space-time evolution of a hot fireball along the transverse beam direction in Pb-Pb collisions with zero impact parameter at SPS and RHIC energies using the hydrodynamic approach. We assume the existence of a first order phase transition from the quark phase to hadrons. Contributions of quarks and mesons to dilepton production are considered separately to enable us to tell whether the quark-gluon plasma actually gets formed. The hadronic source is discussed in detail. The Drell-Yan processes are taken into account as well. We develop further the technique for differential dilepton rate calculation based on the effective interaction Lagrangian approach; it is presented in Appendix C.

5.1 Hydrodynamic model and rate calculation

Most of the physical observables that characterize relativistic heavy ion collisions, such as particle distributions, electromagnetic radiation, and other signs of spatial and temporal evolution of the fireball, are sensitive to the Equation of State of Hadronic matter [53]. In the hydrodynamic description of the QGP, the complete space-time evolution of the system is described by the following variables: energy density ϵ, pressure P, temperature T, and the four-velocity $u^\mu = dx^\mu/d\tau$ in the local rest frame of the medium. The equation expressing local pressure as a function of energy and temperature $P = P(\epsilon, T)$ is the hydrodynamical Equation of State. Hydrodynamics provides a direct relation between the Equation of State and the dynamical evolution of the system.

Quantitative comparison with the SPS data from high energy Pb-Pb collisions suggests the applicability of hydrodynamical concepts already in $\approx 1\, fm/c$ after impact. This point is however still under debate. Many theoretical efforts were invested in the development of the hydrodynamics description of the expanding hot and dense fireball created in ultra-relativistic collisions of heavy nuclei [2,52-63].

In this work we investigate the dilepton yield from the high-energy-density fireball produced at the early stage of the heavy-ion collisions. We assume a system in local thermal equilibrium. It longitudinally expands from QGP, passing first through a mixed phase and then through a hadron phase. In other words, we assume that the matter undergoes a first-order hadronization phase transition in the course of hydrodynamic expansion. Contributions from different sources (QGP, mixed phase, and meson bath) are calculated separately and summed over.

We refer to the J.D.Bjorken's paper [54] regarding the hydrodynamic model formulation and to K.Kajantie, J.Kapusta, L.McLerran, and A.Mekjian [2] regarding the expansion dynamics discussion.

To introduce the hydrodynamic description we start with the conservation law:

$$\partial^{\mu} T_{\mu\nu} = 0, \tag{5.1}$$

where the energy-momentum tensor is defined as

$$T_{\mu\nu} = (\epsilon + P) u_{\mu} u_{\nu} - g_{\mu\nu} P. \tag{5.2}$$

The four-velocity u_{μ} given by:

$$u_{\mu} = \frac{1}{\sqrt{1 - v_r^2}} \left(\cosh \eta, v_r \cos \phi, v_r \sin \phi, \sinh \eta \right), \tag{5.3}$$

where v_r is the transverse (radial) velocity. The space-time rapidity η is defined in a usual way:

$$\eta = \frac{1}{2} \ln \frac{t + z}{t - z}. \tag{5.4}$$

Equation 5.1 for $\nu = 0$ would result in the following equation at zero rapidity :

$$\frac{\partial}{\partial \tau} \left[\frac{\epsilon + P}{1 - v_r^2} - P \right] = - \frac{\partial}{\partial r} \left[\frac{\epsilon + P}{1 - v_r^2} \right] - \frac{\epsilon + P}{1 - v_r^2} \left[\frac{v_r}{r} + \frac{1}{\tau} \right]. \tag{5.5}$$

For numerical purpose, hydrodynamic Equation 5.5 can be rewritten in the form:

$$\frac{\partial}{\partial\tau}T_{00} + \frac{\partial}{\partial r}\left[v_s T_{00}\right] = -\left[T_{00} + P\right]\left[\frac{v_r}{r} + \frac{1}{\tau}\right], \tag{5.6}$$

where for a purpose of simplicity we introduce

$$v_s = \frac{\epsilon + P}{1 - v_r^2}v_r \Bigg/ \left[\frac{\epsilon + P}{1 - v_r^2} - P\right]. \tag{5.7}$$

Equation 5.1 for $\nu = z$ would lead to

$$\frac{\partial}{\partial\tau}\left[\frac{\epsilon + P}{1 - v_r^2}v_r\right] = -\frac{\partial}{\partial r}\left[\frac{\epsilon + P}{1 - v_r^2}v_r^2\right] - \frac{\partial P}{\partial r} - \frac{\epsilon + P}{1 - v_r^2}v_r\left[\frac{v_r}{r} + \frac{1}{\tau}\right], \tag{5.8}$$

which in a similar to Equation 5.6 way can be rewritten as

$$\frac{\partial}{\partial\tau}T_{0r} + \frac{\partial}{\partial r}\left[v_r T_{0r}\right] = -\frac{\partial P}{\partial r} - T_{0r}\left[\frac{v_r}{r} + \frac{1}{\tau}\right]. \tag{5.9}$$

The time evolution of T_{00} and T_{0r} is defined by Equations 5.6 and 5.9. Now the energy density can be readily determined using the following implicit equation

$$\frac{T_{0r}^2}{T_{00} + P(\epsilon)} = T_{00} - \epsilon. \tag{5.10}$$

At this point the evolution of all thermodynamic quantities at different space-time points can be described. The pressure P is determined from the Equation of State. The velocity u^μ is determined from T_{00} and T_{0r}.

Now, once the general formalism is defined, we are able to consider different scenarios for a collision of two heavy nuclei. One can include only light mesons or all possible resonances, assume the presence of a phase transition from QGP to the hadron phase or not. Depending on the choice of the scenario the dynamical evolution of the system will be different [61]. The results obtained can then be compared with the experiment in order to justify the choice.

Now we proceed to calculation of the so-called thermal dilepton contribution to the dilepton emission spectrum. We use the formalism of relativistic kinetic theory. Our final aim is to compare our prediction with the experimental measurements on lepton pair emission. We are interested in several differential rates which can be obtained on the basis of kinetic theory (see Appendix C). Differential rates $dR/dM^2\, d^3\vec{q} = dN/d^4x\, dM^2\, d^3\vec{q}$ are extracted from Equations 2.10 or 2.20 depending on whether we consider a decay of a meson or a two-body reaction taking place in the hot hadronic matter correspondingly.

For the mesonic reactions taking place in a hot hadronic environment the differential dilepton emission rate can be written as (Equation C.6 in Appendix C):

$$E\frac{dR}{dM^2 d^3\vec{q}} = \mathcal{N}\frac{\sigma(M^2)}{4(2\pi)^5 M^2}((M^2 + m_a^2 - m_b^2)^2 - 4M^2 m_a^2) f(E) \qquad (5.11)$$

where $f(E)$ is the occupation probability. The quantum effects in our case are not important but relativistic effects are, hence, we use $f(E) = exp(-\sqrt{p^2 + m^2}/T)$.

Similarly, for the decay processes happening in the hot meson bath the differential rate for each particular type of interaction in the most general form is (Equation C.18 in Appendix C):

$$E\frac{dR}{dM^2 d^3\vec{q}} = \mathcal{N}\int_{E_a^{min}}^{E_a^{max}}\int_{p_+^{min}}^{p_+^{max}} \frac{|\mathcal{M}|^2}{32(2\pi)^6 q^2} dp_+ dE_a f(E_a)\,(1+f(E-E_a)). \quad (5.12)$$

where the limits of integration are similar to Equations C.12 and C.17, derived in Appendix C.

Since we are interested in the space-time history and the cooling of the hadronic fireball, the integration of the emission rates over space-time volume of the reaction is necessary. In the framework of Bjorken's model the volume element can be represented in terms of time t, rapidity of the fluid element y, and transverse coordinate x_T as

$$d^4x = d^2x_T\, dy\, t\, dt. \quad (5.13)$$

If we restrict ourselves to the case of central collisions of equal-mass nuclei (Pb-Pb in our case), the integration over transverse coordinate would give us just a numerical factor $\int d^2x_T = \pi R_A^2$, where R_A is the nuclear radius.

Our rather pragmatic point of view is based on the assumption of first-order phase transition taking place in the course of the space-time evolution of the fireball. Hence the temperature evolves in time as it is shown in Fig. 5.1, where at the very beginning, when the temperature is close to initial T_0, QGP is produced. Then the system adiabatically expands until the temperature drops to T_c. At this stage the nucleation of the hadron phase starts and the system enters the mixed phase. The hadronization continues until there are no quarks left. Then the temperature begins to fall again.

Let us consider the dilepton production step-by-step in time. First of all, let us look

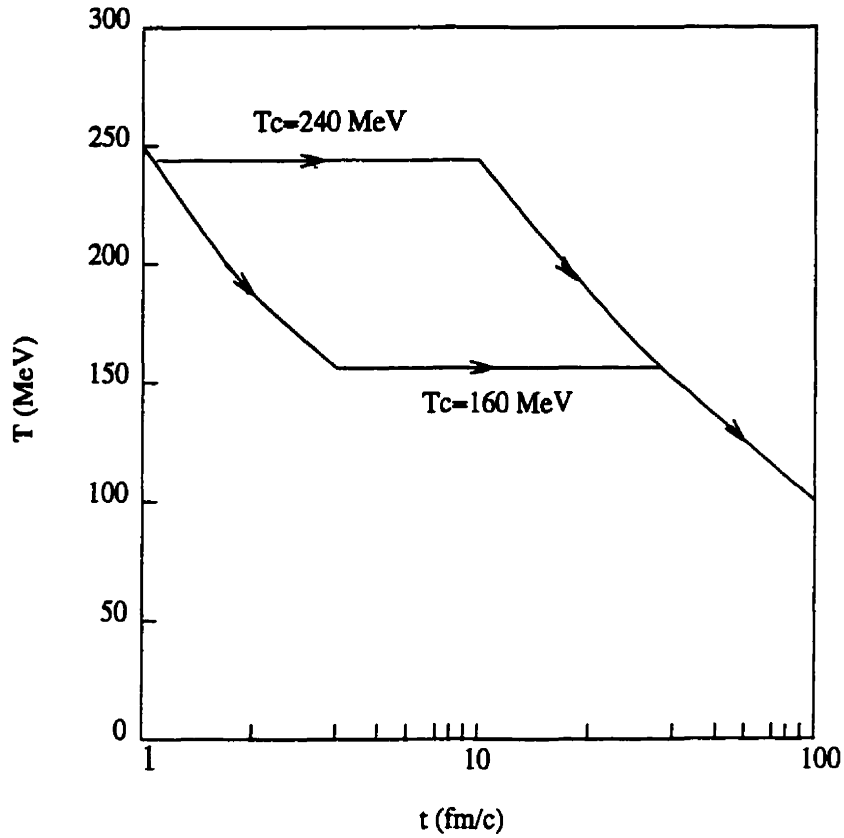

Figure 5.1: The time evolution of the temperature in Bjorken's model for initial condition T_0=250 MeV at $t_0 = 1$ fm/c. Two different values of the critical temperature are represented.

at the quark phase when $T_0 > T > T_c$ and $t_0 < t < t_c$ with T_0 and t_0 being the initial temperature and time. The total number of lepton pairs emitted per unit of rapidity y is [2]:

$$\frac{dN^q}{dy} = 3\pi R_A^2\, t_0^2\, T_0^6 \int_{T_c}^{T_0} dT\, T^{-7}\, R^q(T). \tag{5.14}$$

If m_l can be neglected compared to the temperature, and that is the case even for muons since $T_c > m_\mu$, an analytical integration may be carried out. Taking into account that for e^+e^- production by u and d quarks $R^q(T) = 10/(9\pi^3)\alpha^2 T^4$ [2] the total number of dileptons per unit of rapidity becomes:

$$\frac{dN^q}{dy} = \frac{\alpha^2}{(2\pi)^2} R_A^2 \, F_q \, t_0^2 \, T_0^4 \, [\left(\frac{T_0}{T_c}\right)^2 - 1], \tag{5.15}$$

where the quark form factor is defined as $F_q = N_c(2s+1)^2 \sum_f e_f^2$ (sum is over the different quark flavors).

Next we consider a region along the Maxwell coexistence line. Here the rate as a function of temperature is constant since the temperature is fixed. But one has to account for the fraction of volume occupied by plasma:

$$\frac{dN^q}{dy} = \pi R_A^2 \, R^q(T_c) \int_{t_1}^{t_2} f(t) \, t \, dt, \tag{5.16}$$

where $\int_{t_1}^{t_2} f(t) \, t \, dt = \frac{1}{2}(r-1) f_0^2 t_1^2$ with $r = \frac{37}{3}$ being a ratio of the number of degrees of freedom in the two phases [2]. This result holds even when the system starts in the mixed phase ($T_0 = T_c$, $0 < f_0 < 1$, $t_1 = t_0$) without actually going through the purely quark phase.

The hadronic contribution along the Maxwell coexistence line is analogous to Equation 5.16:

$$\frac{dN^h}{dy} = \pi R_A^2 \, R^h(T_c) \int_{t_1}^{t_2} [1 - f(t)] \, t \, dt \tag{5.17}$$

with $\int_{t_1}^{t_2}[1-f(t)]\,t\,dt = (r-1)[1+\frac{1}{2}(r-2)f_0]\,f_0\,t_1^2$.

At last, on the cooling line, when $T < T_c$, the hadronic contribution is:

$$\frac{dN^h}{dy} = 3\pi R_A^2\, t_0^2\, T_0^6 \int_{T_f}^{T_c} dT\, T^{-7}\, R^h(T). \tag{5.18}$$

In order to obtain the distribution $dN/dy\,dM^2$ one has to introduce the corresponding differential rate (see Equations C.6, C.18 in Appendix C) into Equation 5.18.

5.2 Initial conditions

In order to calculate the yield of the thermal dileptons, the integration over space-time history of the evolving interacting system must be performed. We assume that a thermally and chemically equilibrated quark-gluon plasma is produced in such collisions at a time τ_0, which may be estimated from the condition of isentropic expansion of the plasma [54]:

$$c\,\frac{1}{A_T}\frac{dN}{dy} = 4aT_0^3\tau_0. \tag{5.19}$$

Here dN/dy is the particle rapidity density for the collision, A_T is the transverse area of the colliding system, and for a plasma of massless u, d, and s quarks and gluons, $c = 2\pi^4/(45\zeta(3)) \sim 3.6$ and $a = 42.25\pi^2/90$. We see that once A_T and dN/dy are known, the above relation uniquely relates T_0 to τ_0.

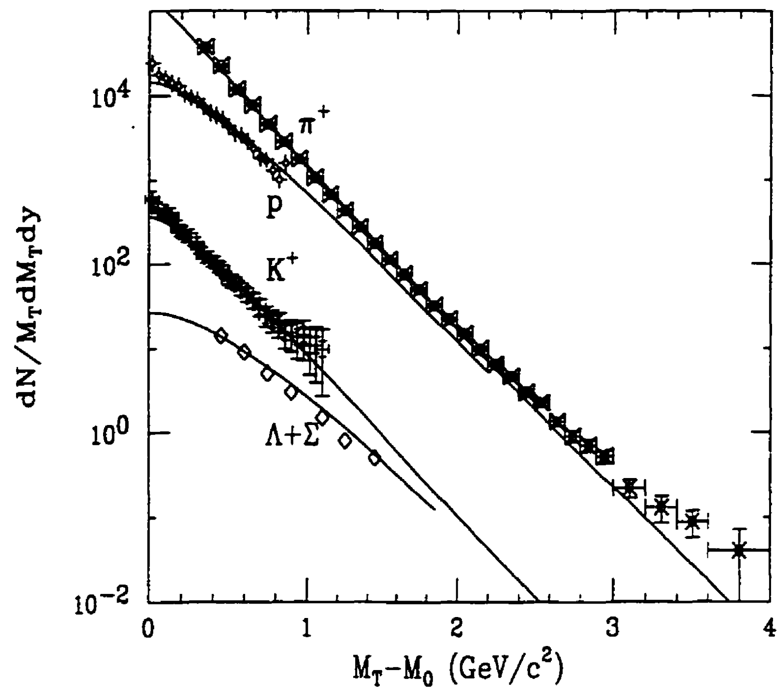

Figure 5.2: Hadronic spectra in central collison of Pb nuclei at SPS energy. The formation time is 0.2 fm/c. The data are from [64].

We assume the plasma to undergo a boost-invariant longitudinal expansion and an azimuthally symmetric radial expansion followed by a transition to a hot hadronic gas consisting of hadrons with $m < 2.5$ GeV in a thermal chemical equilibrium at a transition temperature T_c. We also assume that the coupling between the longitudinal and transverse flows is weak and neglect the transversal variation of all quantities. Once all the quark-matter is converted to the hadronic matter, the hot hadronic system continues to expand until it undergoes a freeze-out at some temperature T_f. The speed of sound in the matter is consistently calculated for all the stages of this evolution and lately used in the equation of state for solving the hydrodynamic equations.

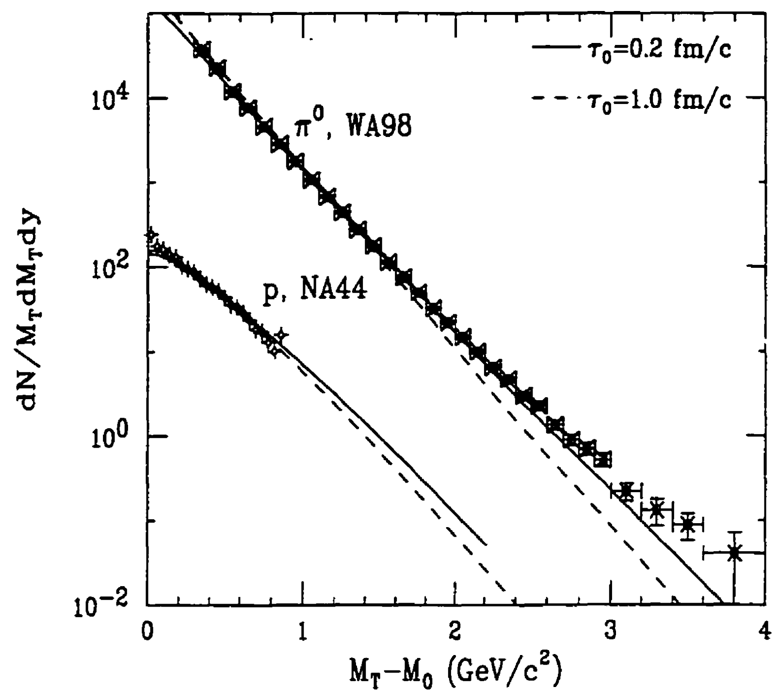

Figure 5.3: Hadronic spectra in central collison of Pb nuclei at SPS energy. The formation time is taken as 0.2 fm/c and 1 fm/c respectively. The data are from [64].

The average particle rapidity density was taken to be 750 for the 10% most central Pb+Pb collisions at the CERN SPS energy. We estimate the average number of participants for the corresponding range of impact parameters ($0 \leq b \leq 4.5$ fm) as about 380 out of the maximum of 416 for a head-on collision. We thus use a mass number of 190 to get the radius of the transverse area A_T of the colliding system and for simplicity neglect its deviations from azimuthal symmetry. As this deviation, measured in terms of the number of participants, is marginal (< 9%) we expect the error involved to be small. We also recall that the azimuthal flow is minimal for central collisions.

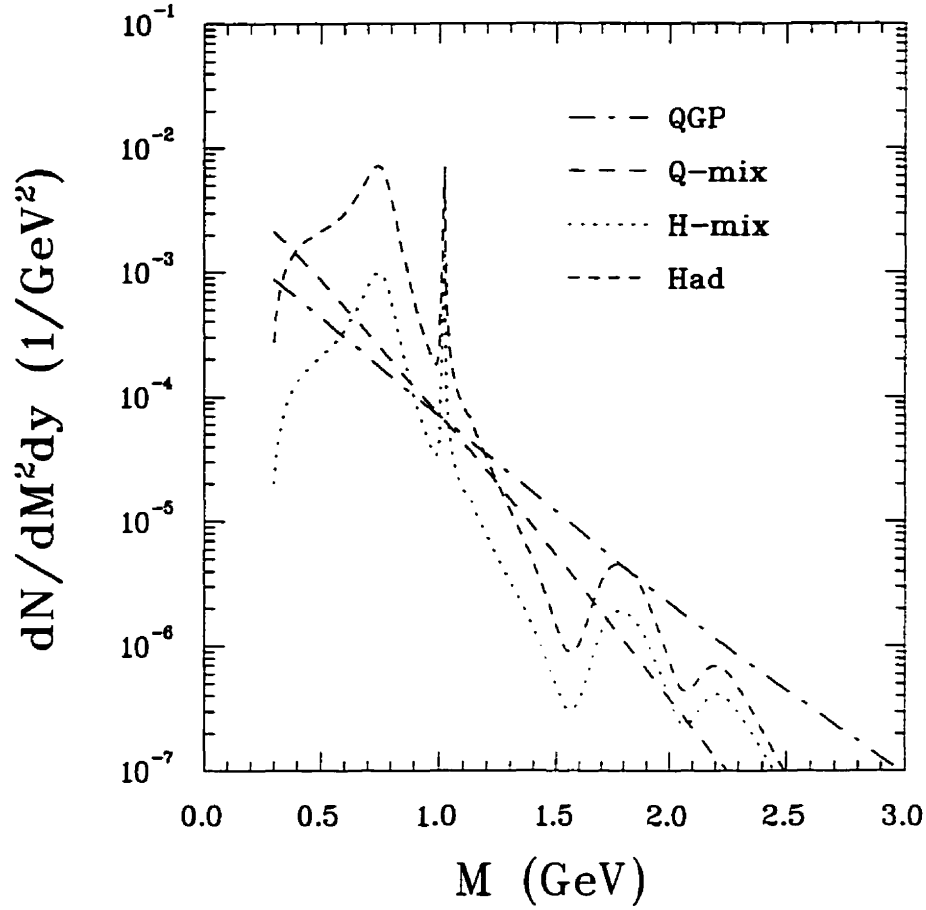

Figure 5.4: Differential rate of dilepton production versus invariant mass of quark phase, hadronic phase, quarks, mixed with hadrons, and hadrons, mixed with quarks for central Pb-Pb 158 AGeV collisions at CERN-SPS. The critical temperature is taken to be T_c =180 MeV, the initial temperature is T_i =330 MeV, and the freeze-out temperature is T_f =120 MeV.

Using the rapidity density observed at SPS energies in central collisions involving lead nuclei, it was shown recently [5] that the formation time of the plasma $\tau_0 = 0.2$ fm/c is consistent with the single photon data. In Figure 5.2 and 5.3 we show our results for hadronic spectra when the formation time is taken 0.2 fm/c and 1 fm/c. Even though a reasonable variation of the initial temperature and the formation time, keeping the corresponding dN/dy fixed, can affect the flow only marginally, we study the consequences of increasing τ_0. We see that the hadronic spectra can not distinguish such variations in the initial conditions, as the flow takes some time to develop. Using Equation 5.19, we get for the initial temperature T_i =330 MeV.

The phase transition is assumed to take place at $T_c = 180$ MeV and the freeze-out at T_f =120 MeV. This value of the critical temperature follows from the recent lattice QCD results which we discuss on Page 2.

Turning to dileptons, we show in Figure 5.4 our results for the quark, hadronic and mixed phases calculated separately. Initial conditions are chosen to fit the experimental setup for central Pb-Pb 158 AGeV collisions at CERN-SPS: $T_c = 180$ MeV, T_i=330 MeV, and T_f =120 MeV.

5.3 Drell-Yan process

In this section we discuss the theory of Drell-Yan production, which is especially important for large values of the invariant mass of lepton pair. The leading order contribution to Drell-Yan process in a nucleus-nucleus collisions is illustrated in Figure 5.5. This process represents the quark-antiquark annihilation of a valence quark and a sea antiquark, producing a virtual photon, which then decays into a pair of

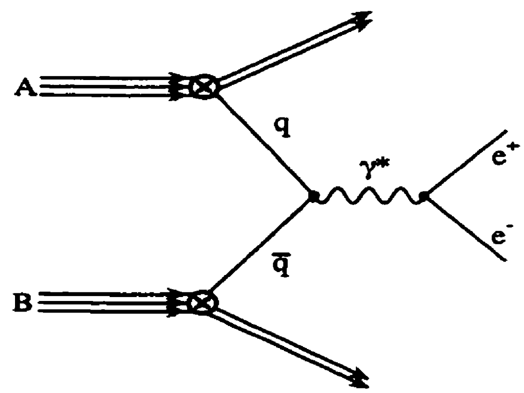

Figure 5.5: The diagram for the Drell-Yan process leading to the production of a dilepton pair.

oppositely charged leptons.

The cross-section for the elementary process

$$q_i\bar{q}_i \rightarrow \gamma^* \rightarrow l^+l^- \tag{5.20}$$

is

$$\frac{d\sigma}{d\Omega}\Big|_{c.m.s.} = \frac{4\alpha^2}{16M^2}\left(\frac{e_q}{e}\right)^2(1+\cos^2\theta), \tag{5.21}$$

which gives after integration

$$\sigma(q\bar{q} \rightarrow l^+l^-) = \frac{4\pi}{3}\frac{\alpha^2}{M^2}\left(\frac{e_q}{e}\right)^2, \tag{5.22}$$

where e_q is a charge of the quark and α is a fine structure constant.

It is useful to introduce the Feynman scaling variable x_F for the dileptons,

$$x_F = \frac{C_z}{\sqrt{s}/2} \tag{5.23}$$

with $C_z = p_z^+ + p_z^-$ as a longitudinal momentum of the lepton pair in the nucleon-nucleon center-of-mass system and $\sqrt{s}$ as the nucleon-nucleon center-of-mass energy.

It is easy to show [1] that the differential cross section of Drell-Yan process in terms of M^2 and x_F in a nucleus-nucleus collision is

$$\frac{d^2\sigma}{dM^2 dx_F} = \frac{4\pi\alpha^2}{9M^2 s} \sum_f^{N_f} \left(\frac{e_q}{e}\right) \frac{q_f^B(x_1)\bar{q}_f^A(x_2) + \bar{q}_f^B(x_1)q_f^A(x_2)}{\sqrt{x_F^2 + 4M^2/s}}, \tag{5.24}$$

where $q_f^{(A,B)}(x)$ and $\bar{q}_f^{(A,B)}(x)$ denote the probability of finding a quark or an antiquark of flavor f in nucleon A or B.

If we express M^2 and x_F in terms of light-cone variables x_1, x_2, which are

$$x_{1,2} = \frac{1}{2}\left(\sqrt{x_F^2 + \frac{4M^2}{s}} \pm x_F\right),$$

$$x_1 - x_2 = x_F, \tag{5.25}$$

$$x_1 x_2 s = M^2,$$

the cross section becomes

$$\frac{d^2\sigma}{dM^2 dx_F} = \frac{4\pi\alpha^2}{9M^2 s} \sum_f^{N_f} \left(\frac{e_q}{e}\right) \frac{q_f^B(x_1)\bar{q}_f^A(x_2) + \bar{q}_f^B(x_1)q_f^A(x_2)}{x_1 + x_2}. \tag{5.26}$$

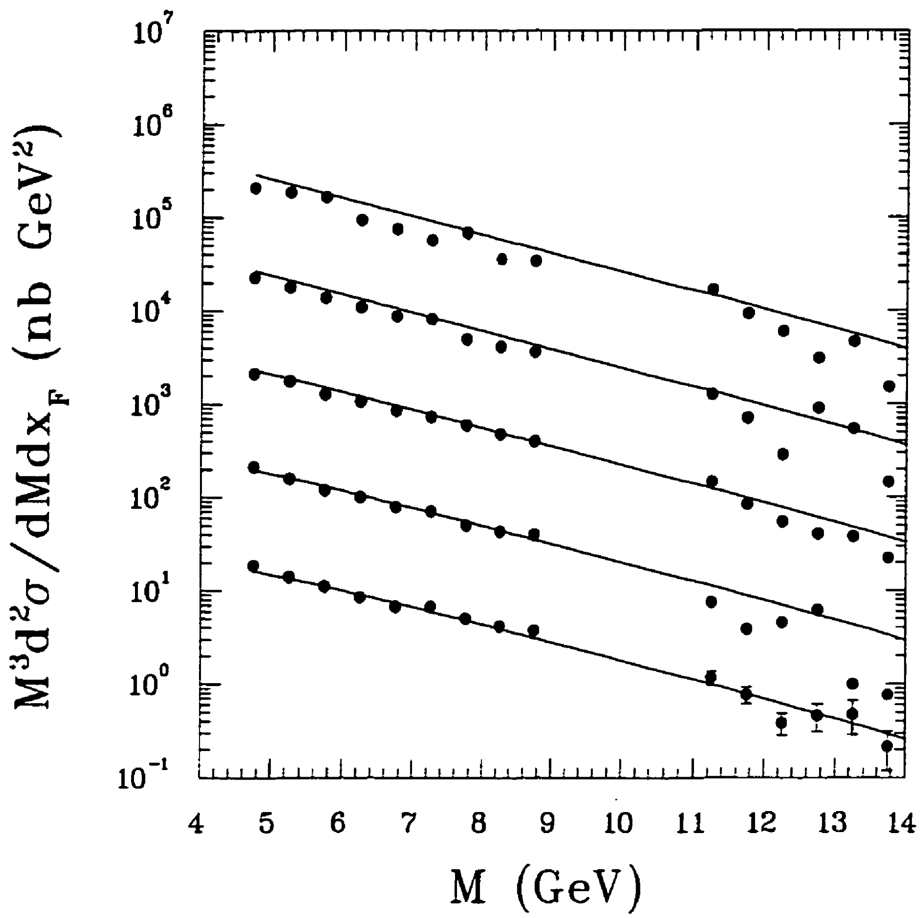

Figure 5.6: Differential cross section of Drell-Yan process as a function of dilepton mass for different Feynman scaling variables $x_F = 0.025 + 0.05 * n$ multiplied by the factor 10^n for n=0,1,2,3,4. Solid curve is our calculated result, points are the data from Fermilab E772 experiment for $pp \rightarrow \mu^+\mu^- X$ at p_{lab}=800 GeV [66].

Consider the collision of two equal nuclei with mass number A and zero impact parameter. The number of emitted lepton pair is given by

$$\frac{dN_{l^+l^-}}{dMdy}\mid_{b=0}= \frac{3}{4\pi(r_0')^2}A^{4/3}\frac{d\sigma_{DY}^{NN}}{dMdY}. \tag{5.27}$$

which in terms of elementary Drell-Yan cross section reads

$$\frac{d^2\sigma_{DY}^{NN}}{dMdy} = K\frac{8\pi\alpha}{9Ms}\sum_{q=u,d,s} e_q^2[q(x_1)\bar{q}(x_2) + \bar{q}(x_1)q(x_2)]. \tag{5.28}$$

Here $r_0' = 1.05\ fm$ and a K-factor accounts for higher order effects.

We follow this ideology in obtaining the leading order Drell-Yan contribution in our analysis. In order to extract information on the parton distribution functions, the cross sections for deep inelastic scattering processes can be measured; from the measured cross sections, the nucleon structure functions can be deduced and the parton distribution functions extracted. A large set of experimental data is available (see, for example, [66, 67]). We employ the recent leading order parameterization from [68] (GRV-94 LO) which requires a K-factor to be 1.5 in order to comply with p-A Drell-Yan data. For a test, let us compare the calculated Drell-Yan yield to the measurements from Fermilab E772 experiment for the reaction $pp \rightarrow \mu^+\mu^- X$ at p_{lab}=800 GeV. The results are represented in Figure 5.6. The comparison illustrates quite a nice agreement between both.

5.4 Comparison with heavy ion experimental data

The NA50 experiment at the CERN SPS studies the muon pair production in nucleus-nucleus collisions with a general purpose to probe the behavior of hot and dense nuclear matter. Since the dimuons generated in the fireball volume interact weakly with the hot surrounding medium, they can escape undisturbed and carry out information about the state of matter where they were generated. The experiment NA50 considers the Pb-Pb and p-A collisions at nucleon-nucleon center of mass energies of 18 GeV and 30 GeV respectively. The setup accepts dimuons in a kinematic range roughly defined as $0.1 < y_{lab} < 1.0$ and $M_T > 1$ GeV. The physics includes signals which probe Quark-Gluon Plasma namely, J/ψ, vector mesons, thermal and Drell-Yan dileptons. The experiment is a continuation, with improved means, of NA38.

For the purposes of theoretical analysis the dilepton mass spectrum can be roughly subdivided in three main regions: the Low Mass Region (LMR) below the ϕ resonance, the Intermediate Mass Region (IMR) between the ϕ and the J/ψ and the High Mass Region (HMR) above the J/ψ. While the HMR is mostly due to the superposition of dimuons from the DY process, dimuons in the LMR and IMR originate from other sources: hadron Dalitz decays, charmed meson semi-leptonic decays, Drell-Yan processes and thermal dileptons coming from the quark-antiquark annihilation and from hadronic matter interaction.

The thermal contribution due to the mesons decays and reactions is one of the most important contribution to the opposite sign (l^+l^-) low and intermediate mass continuum. Due to the high multiplicity in Pb-Pb interactions, its contribution is still important even in the high mass region up to 3.6 GeV, where J/ψ is situated. We plan to prove this assertion in this chapter.

In order to compute the dimuon kinematic variables, the two muon tracks are assigned to the centre of the identified sub-target. The invariant mass M, the rapidity y, the transverse momentum p_T, and the polar angle θ_{CS} in the so-called Collin-Soper reference frame (rest frame of the dimuon) are then calculated.

	$P_{projectile}$	$\sqrt{s}$	y_{cms}	y^*	$\cos\theta_{CS}$
Pb-Pb	158 AGeV	17.22 GeV	2.91	[0.0; 1.0]	[-0.5; 0.5]

Table 5.1: Kinematic cuts imposed on the dimuon kinematic variables.

To eliminate dimuons coming from kinematic regions where the acceptance of the apparatus is very low, kinematic cuts must be applied on the dimuon rapidity y and $\cos\theta_{CS}$.

Table 5.1 lists the kinematic domains within which events are accepted for our case of study. The rapidity in the center of mass reference frame can be obtained from rapidity in the laboratory system, and vice-versa, using the following equation,

$$y_{lab} = y^* + y_{cms}. \tag{5.29}$$

Here y^* is the rapidity in the center of mass reference frame and y_{cms} is the rapidity of the centre of mass system in the laboratory frame; and

$$\cos\theta^+_{CS} = \frac{p_z^+ - \beta_z^{pair} E^+}{[(1 - \beta_z^{pair^2})(M^2/4 - m_\mu^2)]^{1/2}} \tag{5.30}$$

with p_z^+, E^+ and $\beta_z^{pair} = (p_z^+ + p_z^+ -)/(E^+ + E^-)$ are measured in the laboratory frame. Hence, the single-muon tracks in the lab frame lie in the range [24]

$$0.037 \leq \theta^\mu \leq 0.108. \tag{5.31}$$

For the single-muon tracks the absorption effects must be taken into account. The single-muon energies have to satisfy [24]:

$$E_\mu > \begin{cases} E_{cut} + 16000(\theta^\mu - 0.065)^2, & 0.037 \leq \theta^\mu \leq 0.065 \\ E_{cut}, & 0.065 \leq \theta^\mu \leq 0.090 \\ E_{cut} + 13000(\theta^\mu - 0.090)^2, & 0.090 \leq \theta^\mu \leq 0.108 \end{cases} \tag{5.32}$$

Here we take E_{cut} to be 8 GeV as in Ref. [24].

In order to compare our theoretical curve with the experimental data, one must account for the experimental kinematic cuts. The acceptance of the apparatus for a given physical process is defined as the ratio of the numbers of Monte-Carlo reconstructed and generated events

$$A = \left(\int_{M_1}^{M_2} \frac{dN^{rec}}{dM} dM\right) \left(\int_{M_1}^{M_2} \frac{dN^{gen}}{dM} dM\right) \tag{5.33}$$

with the rapidity and $\cos\theta_{CS}$ kinematic cuts have been applied on both distributions.

Monte-Carlo simulations have been carried out in order to compute the corresponding to our experimental setup acceptance ratio A from Equation 5.33. The obtained acceptance ratio is plotted in Figure 5.7.

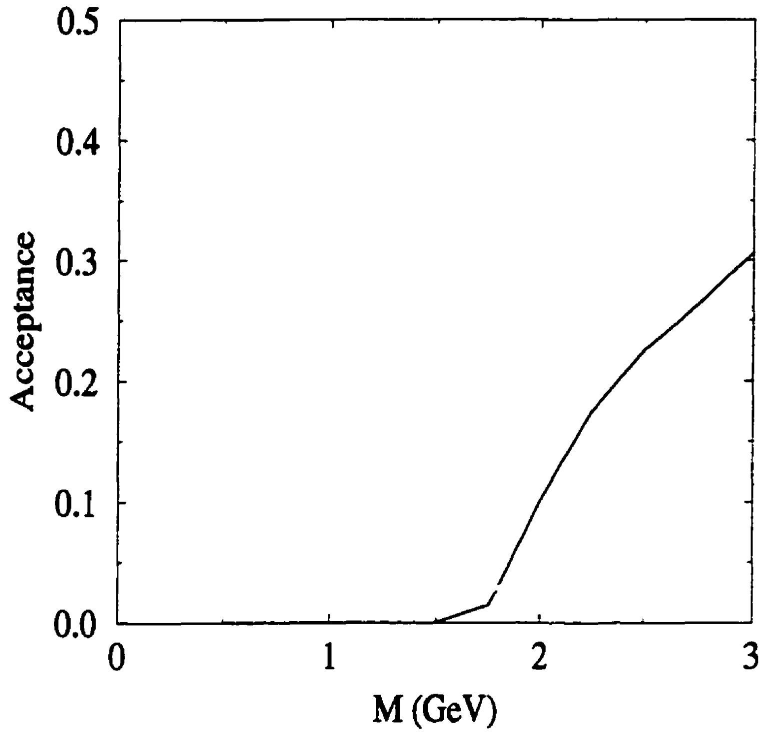

Figure 5.7: The acceptance ratios for NA50 experiment on Pb-Pb 158 AGeV collisions for the transverse momentum p_T=2.5 GeV and rapidity $y = 3.411$.

In the present study various contributions to the dilepton production are included into consideration. Among them the most important are the thermal dileptons, Drell-Yan processes, semi-leptonic decay of charmed hadron pairs, and J/ψ and ψ' contributions. We used the charm decay contribution evaluated by NA50 Collaboration, as was done in [24]. In Figure 5.8 the differential rate of lepton pair production is summed over all most significant sources and compared to experimental points obtained recently by NA50 collaboration [6]. The agreement is quite remarkable! Moreover, the thermal dileptons contribution exactly amounts to 3.6 times the charm decay contribution,

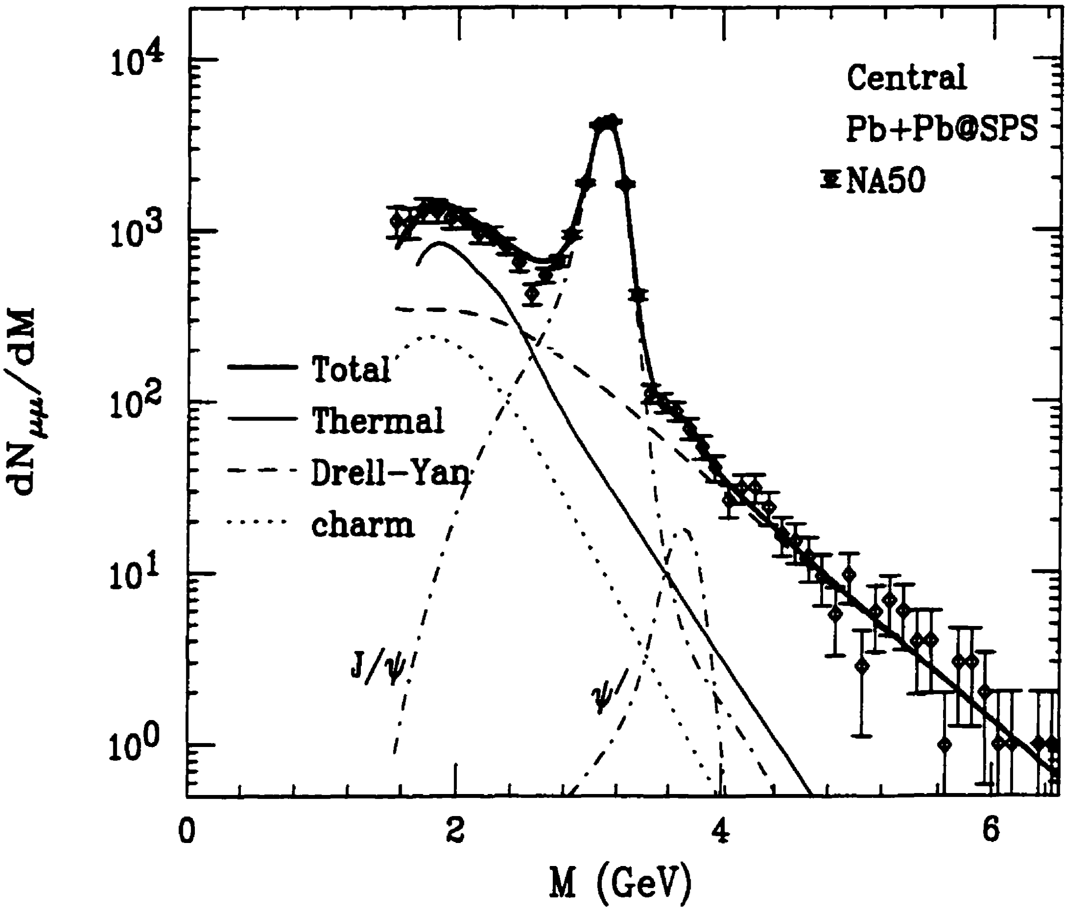

Figure 5.8: IMR dilepton spectrum as a function of invariant mass in comparison to NA50 data from central Pb(158 AGeV)+Pb collisions. The processes contributing to the intermediate mass region are shown: thermal dileptons (solid line), the Drell-Yan lepton pairs (dashed line), the high mass J/ψ and ψ' resonances (dash-dotted line), and semi-leptonic decay of charmed hadron pairs (dotted line). Theoretical curves are calibrated using the acceptance cut as given in the text.

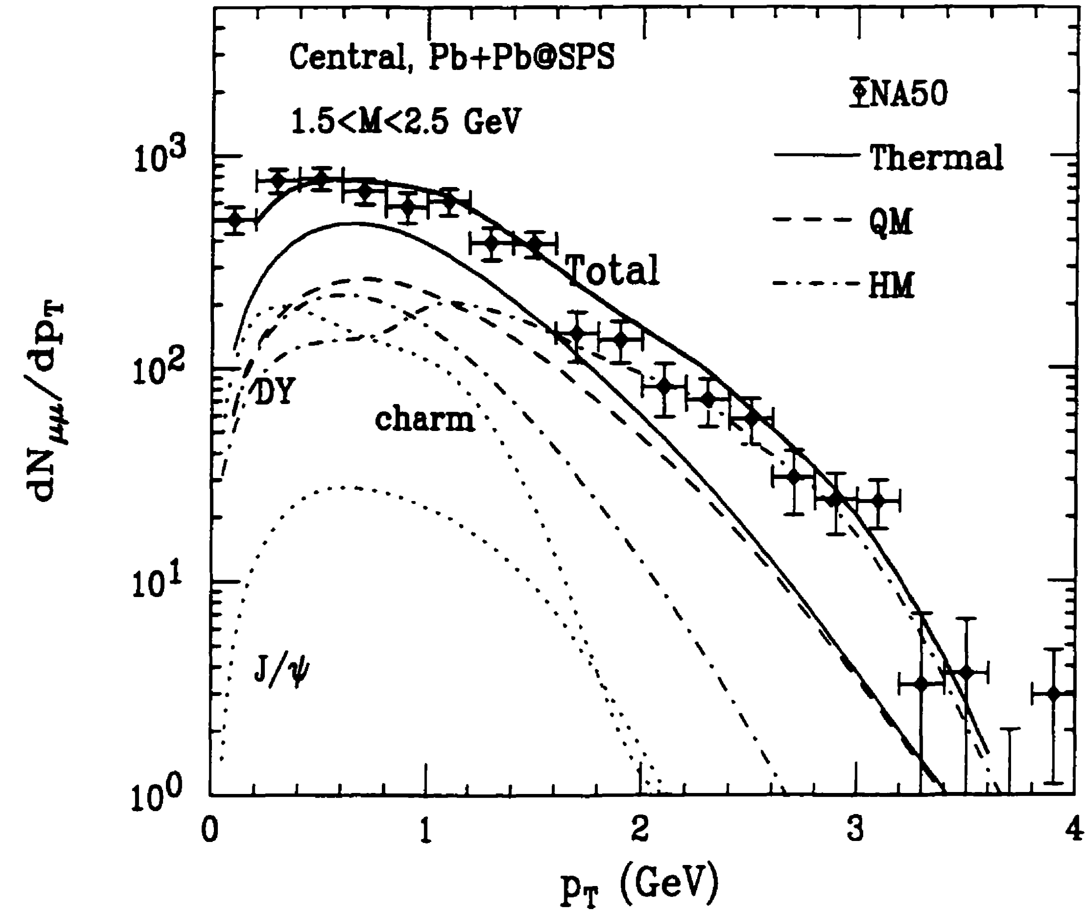

Figure 5.9: IMR dilepton spectrum as a function of transverse momentum in comparison to NA50 data from central Pb(158 AGeV)+Pb collisions. Contributions of the hadron phase and quark phase are shown separately. The charm contribution is accounted for by NA50 Collaboration. Theoretical curves are calibrated using the acceptance cut given in the text.

which, according to NA50 claim [69], was needed to explain the mysterious excess of dileptons in the IMR region. We believe this is a very compelling agreement. In Figure 5.9 the differential rate dN/dp_T of lepton pair production as a function of transverse momentum p_T is plotted along with the experimental points from [6]. Hadronic and quark matter contributions are presented separately as well as the thermal dileptons, charm decay and Drell-Yan process. Once again, the agreement of our calculated total dilepton emission rate with the experimental data on central Pb(158 AGeV)+Pb collisions is quite satisfying. We believe the obtained results can be considered as an encouraging evidence of the plasma formation in ultra-relativistic heavy ion collisions. Of course, further experiments and calculations are needed to put this on a firmer theoretical footing.

5.5 Predictions for the future experiments

The "direct" observation of the quark-gluon plasma may be possible via electromagnetic radiation emitted by the quarks during the hot initial stage. The search for this radiation in the current relativistic heavy-ion experiments at CERN-SPS (WA98, NA45, NA50) is difficult due to high backgrounds from other sources. Prior to our research, recent experimental measurements of the dilepton production conducted by NA38 and NA50 [6] were showing that the sum of the expected sources systematically underestimates the IMR data in the mass region between the ϕ and J/ψ vector mesons. We showed that thermal dileptons may successfully reproduce the excess in the experimental yield even though the predicted electromagnetic radiation rates at the above mentioned temperatures are marginal for detection. While under these conditions it is a great experimental achievement to have obtained positive evidence for a signal, its connection with the predicted "thermal plasma radiation" is not yet firmly established.

This is expected to change at the higher collision energies provided by BNL-RHIC and CERN-LHC. The much higher initial temperatures (up to nearly 1 GeV for Pb-Pb collisions at the LHC have been predicted [70]) and longer plasma lifetimes should facilitate the direct observation of the plasma radiation and lead to the production of additional heavy charm quarks by gluon-gluon scattering in the QGP phase. The much higher initial energy densities which can be reached at RHIC and LHC give us more time until the quarks and gluons hadronize, thus allowing for a quantitative characterization of the quark-gluon plasma and detailed studies of its early thermalization processes and dynamical evolution. Finally, the higher collision energies allow for the production of jets with large transverse momenta, whose leading quarks can be used as "hard penetrating probes" within the quark-gluon plasma. The production of dileptons with intermediate invariant mass in the region between ϕ and J/ψ is widely considered as one of the main tools to measure the "initial" temperature and other thermodynamical characteristics of the matter produced in such experiments [16, 71, 72]. Dilepton measurements are envisaged in particular with the PHENIX and ALICE detector facilities at RHIC and LHC, respectively.

The thermal dilepton signal in the IMR faces a serious background problem. The general expectation is that with increasing beam energy the maximum temperature of matter rises and consequently the thermal dilepton yield grows faster than the Drell-Yan yield. However, with increasing beam energy, a copious production of heavy quarks, resulting in hard initial collisions of partons, also sets in. As a consequence, the correlated semileptonic decays of open charm and bottom mesons yield a dilepton rate exceeding the one from the Drell-Yan process. This can be understood from the following simple arguments. Drell-Yan pairs are produced dominantly via $q\bar{q}$ annihilation, while the open charm and bottom production involves mainly gluons. One can expect an increase of the relative contribution from charm and bottom

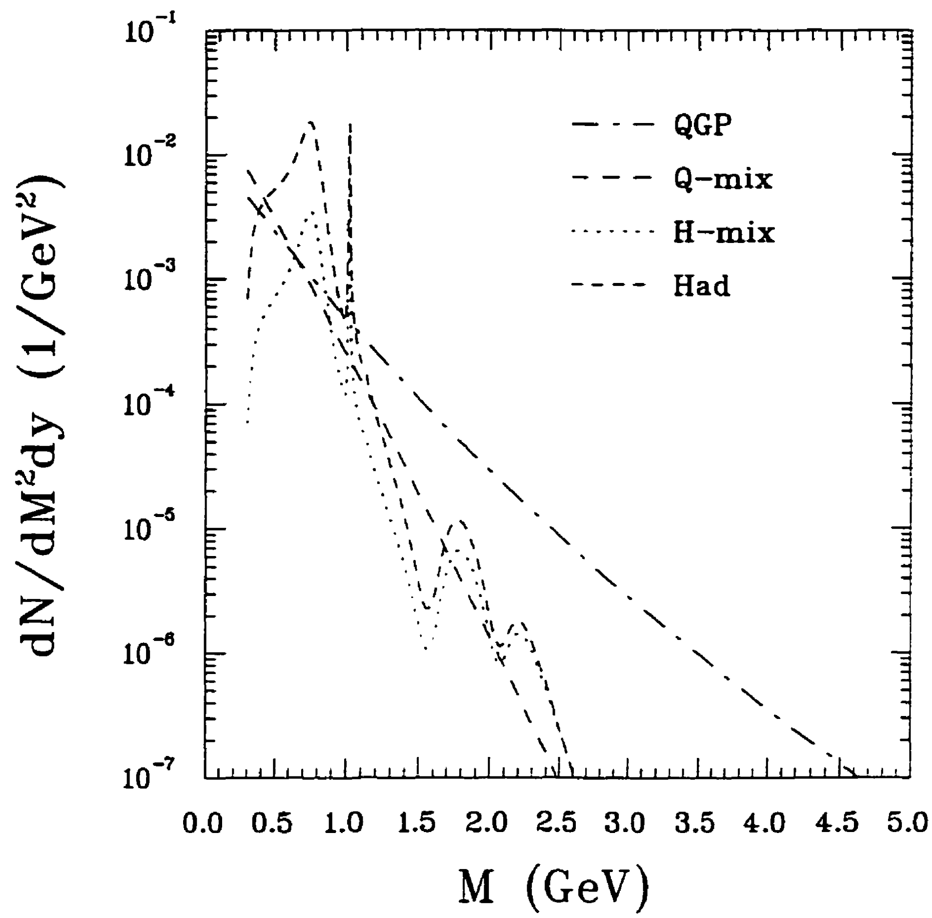

Figure 5.10: Differential rate of dilepton pıoduction from quark phase, hadronic phase, quarks, mixed with hadrons, and hadrons, mixed with quarks, versus invariant mass of lepton pair calculated for the setup of Pb-Pb experiment at RHIC energies. The initial conditions are T_c =180 MeV, T_i =550 MeV, and T_f =120 MeV.

decays into the intermediate mass region of dileptons with increasing beam energy or $\sqrt{s}$. Therefore it is *a priori* not obvious in which energy region one meets the best conditions for observing a thermal dilepton signal from hot deconfined matter. Our work suggests that an observation of the thermal signal seems to be feasible, if the uncorrelated background can be accurately enough removed by like-sign subtraction.

In Figure 5.10 we display our predictions of the thermal dilepton yield. The initial parameters are chosen to fit the planned experiment at BNL-RHIC and discussed in Section 5.2. Compared to the corresponding plot for CERN-SPS experiment (Fig. 5.4), the yield shows strong initial energy dependence. Clearly, as the beam energy increases, the maximum temperature of the fireball rises and consequently the thermal dilepton yield grows.

5.6 Summary

In this chapter we have considered the thermal dilepton spectra from central Pb-Pb collisions at CERN SPS. The applicability of the hydrodynamic approach to the space-time evolution of the fireball and its general formalism have been discussed.

The comparison of the theoretical curve of IMR dilepton spectra to NA50 data from central Pb(158 AGeV)+Pb collisions has been carried out. Experimental acceptance cuts have been accounted for. Theoretical curve was calculated using the acceptance given in the text. The Drell-Yan processes were taken into account as well.

The comparison to the experimental data has shown a remarkable agreement of the theoretical results that were calculated in the assumption that the first-order phase transition from quark phase to hadrons had actually happened. Even more, the NA50 claim [69] has been satisfied: it has been shown that the thermal dileptons contribute exactly 3.6 times the charm decay contribution, as it was required to explain the dilepton excess in IMR region.

Predictions for the future experiments that are on the way at BNL-RHIC and CERN-LHC have been completed for higher energies.

Chapter 6

Summary and Conclusion

This work is about dilepton production from a hot meson gas. Our main motivation for selecting this field of study is the following: The thermal dilepton contribution due to the mesons decays and reactions is one of the most important contributions to the opposite sign (l^+l^-) low and intermediate mass continuum. Since dileptons do not suffer final state interaction, they can be considered as a good probe of what is really happening in the course of ultra-relativistic heavy ion collisions.

The technique we employ in order to conduct our research on mesonic interactions is based on the effective Lagrangian approach. Chapter 2 is devoted to the discussion of the theory of effective interaction Lagrangians of mesons in a hot hadron gas. Since there are parameters in the Lagrangian that cannot be determined from the fundamental theory but must be inferred from the experimental data, we make use of the available experimental data as completely as possible. A complete method for lepton pair production rate calculation, given the interaction Lagrangian for the cases of decaying particle and annihilation processes among mesons is developed.

In Chapter 3 we consider different effective Lagrangians for the $a_1\rho\pi$ interaction in order to estimate lepton pair production rate. The importance of a_1 resonance comes out of the fact that a_1 contribution into the photon production is very large. The analysis shows that the dilepton production differential rates differ significantly depending on the type of strong interaction Lagrangian that is used.

Since in the hot meson environment created in relativistic heavy ion collisions there are processes that constitute greater contribution to the dilepton emission then decaying a_1, it is difficult to get the experimental data on a_1 decay to support our judgment of how "good" the Lagrangian is. Yet special care must be taken respecting a type of the interaction Lagrangian. Our choice must be based on comparison with the experimentally measured hadronic properties.

Among known $a_1 \to \pi e^+e^-$ interaction Lagrangians, Gomm, Kaymakcalan, Schechter Lagrangian (parameter set 2) is proven to fit experimental data better then the others.

We also introduce in this chapter a new form of $b_1\omega(\phi)\pi$ effective Lagrangian and calculate the dilepton production differential rate for the $b_1 \to \omega(\phi)\pi \to \gamma\pi \to e^+e^-\pi$ decay.

In Chapter 4 we have conducted the systematic research on the light meson contribution to the dilepton emission in ultra-relativistic heavy ion collisions for the temperature T=150 MeV. The results are used for the further development of lepton pair production rate calculations using hydrodynamic model of heavy ion collisions.

The most contributing decays and reactions among all allowed by the conservation laws are calculated and summed for intermediate (up to M =3 GeV) invariant mass dileptons.

We have confirmed that in the region of invariant masses below ρ-meson rest mass (LMR), the ω-meson decay is a dominant contribution. At invariant masses above 1.0 GeV, the contribution from light meson decays sharply drops off due to their insufficient mass, and the meson two-body reactions give rise to the thermal dilepton production.

We compare the total dilepton rate to the recent data obtained using the collection of spectral functions which are extracted from e^+e^- annihilation and τ lepton decay data by Z.Huang [26] in order to justify that our analysis accounts for all the important channels. His analysis was concerned with summing up the largest possible amount of channels that will produce dileptons. Our claim is: the selected set of chosen mesonic reactions and decays is the collection of the most significant contributions to the thermal dilepton emission and the remaining contributions could be simply neglected. Those could include many-body reactions, like three-particle initial states, for example. Once having established that, we turn to IMR where the signals of quark-gluon plasma formation are expected.

In Chapter 5 we develop the technique to calculate the thermal dilepton spectrum from central heavy ion collisions at ultra-relativistic energies in IMR region. The applicability of the hydrodynamic approach to the space-time evolution of the collision fireball and its general formalism are discussed.

The comparison of the theoretical curve of intermediate invariant mass dilepton spectrum to NA50 data from central Pb(158 AGeV)+Pb collisions is carried out. Experimental acceptance cuts are computed and accounted for. We calculate the theoretical curve using the acceptance cuts as given in the text.

The comparison to the experimental data shows a remarkable agreement with the theoretical results that are calculated within the assumption that the first-order phase transition from quark phase to the hadrons has actually happened. Moreover, the thermal dileptons contribution is shown to be exactly 3.6 times the charm decay contribution. The NA50 collaboration claim [69], which is required to explain the dilepton excess in IMR region, can be rephrased as a statement that supports the importance of meson reactions. We believe the obtained results can be considered as an encouraging evidence of the plasma formation in ultra-relativistic heavy ion collisions.

Predictions for the future experiments, that are on the way, are completed for BNL-RHIC and CERN-LHC energies.

The technique for differential dilepton rate calculations based on the effective interaction Lagrangian approach is developed in Appendix C.

In the light of the future research, further dilepton data will be taken by the PHENIX experiment at RHIC (advancing to a new energy frontier) as well as by the precision experiment HADES at GSI. Thus electromagnetic observables are expected to continue contributing to the progress in our understanding of strong interaction physics.

Appendix A

Landsberg formula derivation

We want to calculate the effective mass spectrum for the leptonic pair in the decay $a \to b\ l^+l^-$ normalized to the width of the corresponding radiative $a(k) \to b(p)\gamma(q)$ decay. In [43] the formula is said to be derived for the amplitude of the process of the form

$$\mathcal{M}_{a\to b\gamma} = 4\pi\alpha i[f_{ab}(q^2)\epsilon^{\alpha\beta\gamma\delta}p_\alpha q_\beta \epsilon_\gamma] \cdot \frac{1}{q^2} \cdot [\bar{u}\gamma_\delta u] \tag{A.1}$$

where $f_{ab}(q^2)$ is the form factor of the $a \to b$ transition, $\frac{1}{q^2}$ is photon propagator, $\bar{u}\gamma_\delta u$ is leptonic current, ϵ_γ is an a particle polarization and $\varepsilon^{\alpha\beta\gamma\delta}$ is antisymmetric unity tensor.

Let us now consider the most general form of the amplitude for the process $a(k) \to b(p)\rho(q) \to b(p)\gamma(q)$. It may be written in the form

$$\mathcal{M}_{a\to b\gamma} = J_\mu(q)\epsilon^\mu(q) \tag{A.2}$$

where $J_\mu(q)$ is the hadronic electromagnetic current that includes all the information about $a-b-\rho$ interaction and $\rho-\gamma$ coupling and must be a function of off-shell particle momentum involved in the reaction. $\epsilon^\mu(q)$ is the photon polarization vector.

It leads to the Lorenz-invariant squared amplitude as simple as $|\mathcal{M}_{a\to b\gamma}|^2 = -J^2(q)$. Inserting the result into kinematic expression for the partial decay rate [36]

$$d\Gamma_{a\to b\gamma} = \frac{1}{32\pi^2}|\mathcal{M}_{a\to b\gamma}|^2\frac{|\vec{p}|}{m_a^2}d\Omega \tag{A.3}$$

with $d\Omega$ as a solid angle of b particle, we get the following result for the total radiative decay width

$$\Gamma_{a\to b\gamma} = \frac{1}{16\pi}|\mathcal{M}_{a\to b\gamma}|^2\frac{(m_a^2-m_b^2)}{m_a^3} = \frac{-J^2(0)}{16\pi m_a^3}(m_a^2-m_b^2) \tag{A.4}$$

where m_a, m_b are the masses of the a,b particles correspondingly and the photon is real and, hence, $q^2=0$.

Let us now move on to the next step in our derivation and consider process

$$a(k)\to b(p)\rho(q)\to b(p)\gamma(q)\to b(p)l^+(p_+)l^-(p_-).$$

We can write the amplitude in the same way as we did for the radiative $a(k)\to b(p)\gamma(q)$ decay:

$$\mathcal{M}_{a\to bl^+l^-} = J_\mu(q)\frac{-g^{\mu\nu}}{q^2}eu(p_+)\gamma_\nu\bar{v}(p_-) = J_\mu(q)\frac{e}{q^2}u(p_+)\gamma^\mu\bar{v}(p_-) \tag{A.5}$$

Then Lorenz-invariant squared amplitude will be

$$\begin{aligned}|\mathcal{M}_{a\to bl^+l^-}|^2 &= \frac{e^2}{q^4}J^\mu(q)J^{\mu'}(q)4(p_{+\mu}p_{-\mu'} + p_{-\mu}p_{+\mu'} - g_{\mu\mu'}(p_+\cdot p_-)) = \\ &= \frac{4e^2}{q^4}\{2(J(q)\cdot p_+)(J(q)\cdot p_-) - J^2(q)(p_+\cdot p_-)\}.\end{aligned} \tag{A.6}$$

Using the hadronic electromagnetic current conservation $J(q)\cdot q = 0$, for the frame where $\vec{q} = \vec{p}_+ + \vec{p}_- = 0$ (rest frame of lepton pair) we can write $J_0(q) = 0$, $J^2(q) = -|\vec{J}(q)|^2$ and $J(q)\cdot p_- = -J(q)\cdot p_+ = \vec{J}(q)\cdot\vec{p}_- = -\vec{J}(q)\cdot\vec{p}_+$. Hence,

$$\begin{aligned}|\mathcal{M}_{a\to bl^+l^-}|^2 &= \frac{4e^2}{q^4}\{-2(\vec{J}(q)\cdot\vec{p}_+)^2 - J^2(q)(p_+\cdot p_-)\} = \\ &\frac{4e^2}{q^4}\{2(-|\vec{J}(q)|^2)|\vec{p}_+|^2\cos^2\Theta_+^* - J^2(q)(p_+\cdot p_-)\}.\end{aligned} \tag{A.7}$$

Here Θ_+^* is the angle of $\vec{p}_+$ in the rest frame of lepton pair.

Now for simplicity of our calculations we restrict our discussion to the case of dielectrons only and assume their masses to be negligibly small. Then in the rest frame of lepton pair the invariant mass of the pair is $M^2 = q^2 = (p_+ + p_-)^2 = 2p_+\cdot p_- = (|\vec{p}_+| + |\vec{p}_-|)^2 = 4|\vec{p}_+|^2$. Finally we come to the formula

$$|\mathcal{M}_{a\to be^+e^-}|^2 = \frac{2e^2}{M^2} J^2(q)(\cos^2\Theta_+^* - 1). \tag{A.8}$$

To calculate the differential width of three-body decay let us consider the well known equation [36]

$$\frac{d\Gamma_{a\to be^+e^-}}{dM^2} = \frac{1}{(2\pi)^5}\frac{1}{16M^2}|\mathcal{M}_{a\to be^+e^-}|^2|\vec{p}_+^*|\,|\vec{p}|d\Omega_+^* d\Omega_b, \tag{A.9}$$

where $(|\vec{p}_+^*|, \Omega_+^*)$ is the momentum of the lepton in the rest frame of dilepton pair, and Ω_b is the angle of particle b in the rest frame of decaying particle a. Integrating over Ω_+^* and Ω_b we can write

$$\frac{d\Gamma_{a\to be^+e^-}}{dM^2} = \frac{-e^2 J^2(q)}{96\pi^3 M^2}\frac{|\vec{p}|}{m_a^2}. \tag{A.10}$$

Let us now combine the equation A.4 and equation A.10 and calculate the ratio of differential decay width of $a \to be^+e^-$ to the radiative decay width.

After all algebra using

$$|\vec{p}| = \frac{[(m_a^2 - (M+m_b)^2)(m_a^2 - (M-m_b)^2)]^{1/2}}{2m_a}. \tag{A.11}$$

we finally obtain

$$\frac{d\Gamma_{a\to be^+e^-}}{dM^2} = \frac{\alpha}{3\pi M^2}\frac{J^2(M)}{J^2(0)}\frac{[(m_a^2-(M+m_b)^2)(m_a^2-(M-m_b)^2)]^{1/2}}{m_a^2-m_b^2}\Gamma_{a\to b\gamma}. \quad \text{(A.12)}$$

where $\alpha = e^2/4\pi$ is a fine structure constant.

To check the consistency of our result with the formula

$$\frac{d\Gamma_{a\to be^+e^-}}{dM^2} = \frac{\alpha}{3\pi M^2}\frac{[(m_a^2-(M+m_b)^2)(m_a^2-(M-m_b)^2)]^{3/2}}{(m_a^2-m_b^2)^3} \times \quad \text{(A.13)}$$

$$\times \frac{|f_{ab}(q^2)|^2}{|f_{ab}(0)|^2}\ \Gamma_{a\to b\gamma}$$

given in [43] let us consider the explicit form of hadronic current proposed by L.G.Landsberg:

$$J^\mu(q) = 4\pi\alpha i f_{ab}(q^2)\varepsilon^{\alpha\beta\gamma\mu}p_\alpha q_\beta \epsilon_\gamma(k). \quad \text{(A.14)}$$

In such a case for random value of q hadronic current squared is

$$J^2(q) = -\frac{e^2}{2}((m_a^2+M^2-m_b^2)^2 - 4m_a^2m_b^2)|f_{ab}(q^2)|^2. \quad \text{(A.15)}$$

Substituting the ratio of $J^2(q)/J^2(0)$ into the equation A.12 we get the result which is in complete accordance with the Landsberg formula. Equation A.12 transforms into

$$\lim_{M^2 \to 0} \frac{d\Gamma_{a \to be^+e^-}}{dM^2} = \frac{\alpha}{3\pi M^2} \Gamma_{a \to b\gamma}. \tag{A.16}$$

in the limit of low invariant mass of lepton pair. Easy to see that since

$$\lim_{M^2 \to 0} \frac{J^2(M)}{J^2(0)} = 1 \tag{A.17}$$

this relation is valid for any kind of interaction.

Appendix B

D/S ratio

In this Appendix we show the calculation of the D/S ratio for $a_1 \to \rho\pi$ decay.

Let us start by an axialvector - pseudoscalar - vector vertex function of the type

$$\Gamma^{\mu\nu} = -i\, f\, g^{\mu\nu} - i\, g\, p^\mu q^\nu. \tag{B.1}$$

In the above, q^μ and p^μ are four-momenta for the a_1 and the ρ respectively. The π four-momentum is k^μ. Four-momentum conservation reads $q^\mu = p^\mu + k^\mu$.

We also use standard helicity representation for the polarization vectors,

$$\begin{aligned} \epsilon(\lambda = \pm 1) &= 1/\sqrt{2}\,(0, 1, \pm i, 0) \\ \epsilon(\lambda = 0) &= 1/m^2\,(|\,\vec{p}\,|, 0, 0, E). \end{aligned} \tag{B.2}$$

Polarization vectors satisfy the normalization and transversality conditions:

$$\epsilon(\lambda) \cdot \epsilon^*(\lambda') = -\delta_{\lambda\lambda'}, \tag{B.3}$$

$$\epsilon \cdot p = 0. \tag{B.4}$$

The entire amplitude then looks like

$$\mathcal{M} = -i(f\, \epsilon(\lambda_a) \cdot \epsilon^*(\lambda_\rho) + g\, (\epsilon(\lambda_a) \cdot p)\, (\epsilon^*(\lambda_\rho) \cdot q)). \tag{B.5}$$

The amplitude is diagonal in the helicity basis. Expanding, (and omiting an overall delta-function $\delta_{\lambda_a}^{\lambda_\rho}$)

$$\mathcal{M} = -i \left[\left(-\delta_{\lambda_a}^{+1} - \delta_{\lambda_a}^{-1} - \delta_{\lambda_a}^{0} \frac{E_\rho}{m_\rho} \right) f - g\, \delta_{\lambda_a}^{0} \frac{m_a}{m_\rho} \mid \vec{p} \mid^2 \right]. \tag{B.6}$$

Here E_ρ and $\vec{p}$ are the energy and three-momentum of the ρ, in the frame of a_1.

On the other hand, one can expand the amplitude in spherical harmonics [74]

$$\mathcal{M} = i\, f_{a\rho\pi}^{S}\, \delta_{s_a}^{s_\rho}\, Y_{00}(\Omega_K) \,+\, i\, f_{a\rho\pi}^{D} \sum_{m_L} (1\; 2\; s_\rho\; m_L \mid 1\; s_a)\, Y_{2m_L}(\Omega_K), \tag{B.7}$$

where the Clebsch-Gordan coefficient has the form $(j_1\; j_2\; m_1\; m_2 \mid J\; M)$. The spin projections along the z axis are s_ρ and s_a. Working in the rest frame of the a_1, we find that when $\theta = 0$ in Ω_k (i.e. the ρ and π are moving in the positive and negative z direction), only $Y_{20} \neq 0$. Also, $s \to \lambda$. Matching Equation B.6 and B.7 in terms of their λ_a content, we obtain for $\lambda_a = 1$,

$$(f^S + f^D/\sqrt{2}) = \sqrt{4\pi}\, f, \tag{B.8}$$

and for $\lambda_a = 0$,

$$(f^S - \sqrt{2}\, f^D) = \sqrt{4\pi}\,(\, f\, \frac{E_\rho}{m_\rho} + g\, \frac{m_a}{m_\rho} \mid \vec{p} \mid^2). \tag{B.9}$$

Solving for f^S and f^D, we get

$$f^S = \frac{\sqrt{4\pi}}{3m_\rho}\,(\, f\,(E_\rho + 2m_\rho) + g\, m_a \mid \vec{p} \mid^2), \tag{B.10}$$

$$f^D = -\frac{\sqrt{8\pi}}{3m_\rho}\,(\, f\,(E_\rho - 2m_\rho) + g\, m_a \mid \vec{p} \mid^2) \tag{B.11}$$

The D/S ratio then consists of f^D/f^S.

Appendix C

Differential dilepton rate

We want to develop the formalism of dilepton rate calculation such that the space-time evolution of the hot and dense fireball created in heavy ion collisions can be considered.

The quantity that appears suitable for the purpose is $EdR/dM^2d^3\vec{q}$, where M and $\vec{q}$ are the invariant mass and the three-momentum of lepton pair correspondingly, and $E = \sqrt{M^2 + |\vec{q}^2|}$.

Consider, first, the mesonic reactions taking place in a hot hadronic environment. For the processes $\mathbf{a} + \mathbf{b} \rightarrow \mathbf{e}^+\mathbf{e}^-$ (see Figure 2.2) the differential dilepton emission rate can be written as

$$E\frac{dR}{dM^2d^3\vec{q}} = \mathcal{N}E\int\frac{d^3\vec{p}_a}{2E_a(2\pi)^3}\frac{d^3\vec{p}_b}{2E_b(2\pi)^3}f(E_a)\,f(E_b)\,\sigma(M^2)4\,E_aE_b\,v_{rel}$$

$$\times\delta(M^2-(p_+ + p_-)^2)\,\delta^3(\vec{q}-\vec{p}_a-\vec{p}_b)$$

where the term $4E_aE_bv_{rel}=\sqrt{((M^2-m_a^2-m_b^2)^2-4m_a^2m_b^2)}$ is the Lorentz invariant. Let us recall, that the cross section of the reaction $\sigma(M^2)$ is also the Lorentz invariant. Hence, the desired quantity becomes simply proportional to

$$E\frac{dR}{dM^2d^3\vec{q}}\sim I=\int\frac{d^3\vec{p}_a}{E_a}\frac{d^3\vec{p}_b}{E_b}f(E_a)\,f(E_b)\delta(M^2-(p_+ + p_-)^2)\,\delta^3(\vec{q}-\vec{p}_a-\vec{p}_b) \quad \text{(C.1)}$$

with the corresponding numerical factor depending only upon invariant mass of lepton pairs.

Using spherical symmetry in momentum space and typical mathematical methods of handling the phase integrals, the integral I can be simplified to the form

$$I=2\pi\int\frac{p_a dE_a d(\cos\theta)}{E_b}f(E_a)\,f(E_b) \quad \text{(C.2)}$$

with $E_a=\sqrt{p_a^2+m_a^2}$. E_b is now a function of E_a and the angle θ between particles a and b in the laboratory frame of reference $E_b=\sqrt{m_b^2+q^2+p_a^2+2qp_a\cos\theta}$.

Easy to show that the delta-function can be transformed to the form

$$\delta(E^2-(E_a+E_b)^2)=\frac{\delta(\cos\theta-\cos\theta_0)E_b}{2qp_aE}, \quad \text{(C.3)}$$

$$\cos\theta_0=\frac{-2EE_a-(M^2+m_a^2-m_b^2)}{2qp_a}.$$

Then, after the integration, the expression for I will be transformed to

$$I = \frac{\pi}{qE} f(E)(E_a^{max} - E_a^{min}) \tag{C.4}$$

and E_a^{max} and E_a^{min} are the limits of integration and can be determined from the requirement $|\cos\theta| < 1$. We will have

$$E_a^{max} - E_a^{min} = \frac{q\sqrt{(M^2 + m_a^2 - m_b^2)^2 - 4M^2 m_a^2}}{M^2} \tag{C.5}$$

and the final expression for the differential dileptons production rate will be

$$E\frac{dR}{dM^2 d^3\vec{q}} = \mathcal{N}\frac{\sigma(M^2)}{4(2\pi)^5 M^2}((M^2 + m_a^2 - m_b^2)^2 - 4M^2 m_a^2) f(E). \tag{C.6}$$

Consider now the calculation of the same quantity for the decay processes happening in the hot meson bath. For $\mathbf{a} \to \mathbf{b}\mathbf{e}^+\mathbf{e}^-$ (see Figure 2.1) the differential lepton pair production rate is represented as

$$E\frac{dR}{dM^2 d^3\vec{q}} = \mathcal{N}\int \frac{m_a}{E_a} E \frac{d\Gamma}{dM^2 d^3\vec{q}} \frac{d^3k}{(2\pi)^3} f(E_a)\,(1 + f(E_b)). \tag{C.7}$$

Evaluate, first, the differential width of the decay. From the definition [36]

$$\frac{d\Gamma}{dM^2 d^3\vec{q}} = \int \frac{|\mathcal{M}|^2}{2m_a} \frac{d^3\vec{p}}{2E_b(2\pi)^3} \frac{d^3\vec{p}_+}{2E_+(2\pi)^3} \frac{d^3\vec{p}_-}{2E_-(2\pi)^3} (2\pi)^4$$

$$\times\,\delta^4(k-p-p_+-p_-)\,\delta(M^2-(p_++p_-)^2)\,\delta^3(\vec{q}-\vec{p}_+-\vec{p}_-) \tag{C.8}$$

Integrating over $\vec{p}_-$ and $\vec{p}$ consequentely the expression is transformed to the form

$$\begin{aligned}\frac{d\Gamma}{dM^2 d^3\vec{q}} &= \int \frac{|\mathcal{M}|^2}{m_a}\frac{d^3\vec{p}_+}{(2\pi)^6 2E_+ 2E_b 2E_-} \\ &\quad \times \pi\,\delta(M^2-2p_+(p_++p_--qx))\,\delta(E_a-E_b-p_+-p_-),\end{aligned} \tag{C.9}$$

where $E_- = p_- = \sqrt{q^2+p_+^2-2qp_+x}$ ($x=\cos\theta$ with θ being an angle between $\vec{p}_+$ and $\hat{z}$, if $\hat{z}$ is chosen along $\vec{q}$) and $E_b = \sqrt{p^2+m_b^2} = \sqrt{m_b^2+k^2+q^2-2kqy}$ ($y=\cos\theta'$ with θ' being an angle between $\vec{k}$ and $\hat{z}$).

Writing the angular integration explicitly we find

$$\begin{aligned}\frac{d\Gamma}{dM^2 d^3\vec{q}} &= \int \frac{|\mathcal{M}|^2}{(2\pi)^4 16 m_a}\frac{p_+ dp_+ dx}{2E_b\sqrt{q^2+p_+^2-2qp_+x}} \\ &\quad \times \delta(M^2-2p_+(p_++\sqrt{q^2+p_+^2-2qp_+x}-qx))\,\delta(E_a-E_b-p_+-\sqrt{q^2+p_+^2-2qp_+x})\end{aligned} \tag{C.10}$$

To make use of the delta-functions we replace

$$\delta(M^2-2p_+(p_++\sqrt{q^2+p_+^2-2qp_+x}-qx)) = \frac{\delta(x-x_0)\sqrt{q^2+p_+^2-2qp_+x}}{2qp_+(p_++\sqrt{q^2+p_+^2-2qp_+x})} \tag{C.11}$$

with $x_0 = (2p_+E - M^2)/2p_+q$. We can also compute the limits of integration over p_+ restricting ourselves to $| x_0 | \leq 1$:

$$p_+^{max} = \frac{M^2}{2(E-q)} \qquad \text{and} \qquad p_+^{min} = \frac{M^2}{2(E+q)}. \tag{C.12}$$

It will lead us to

$$\frac{d\Gamma}{dM^2 d^3\vec{q}} = \int_{p_+^{min}}^{p_+^{max}} \frac{| \mathcal{M} |^2}{(2\pi)^4 32 m_a} \frac{dp_+}{qEE_b} \delta(E_a - E_b - E). \tag{C.13}$$

Let us now come back to the differential rate calculations. Collecting everything together we will have

$$E\frac{dR}{dM^2 d^3\vec{q}} = \mathcal{N} \int \frac{| \mathcal{M} |^2}{32(2\pi)^6} \frac{dp_+ k dE_a dy}{q\sqrt{m_b^2 + k^2 + q^2 - 2kqy}} \tag{C.14}$$

$$\times \; f(E_a)\left(1 + f(\sqrt{m_b + k^2 + q^2 - 2kqy})\right)$$

$$\times \; \delta(E_a - \sqrt{m_b + k^2 + q^2 - 2kqy} - E). \tag{C.15}$$

Delta-function is transformed as

$$\delta(E_a - \sqrt{m_b^2 + k^2 + q^2 - 2kqy} - E) = \frac{\delta(y - y_0)\sqrt{m_b^2 + k^2 + q^2 - 2kqy}}{kq} \tag{C.16}$$

with $y_0 = (m_b^2 + k^2 + q^2 - (E_a - E)^2)/2kq$. The limits of integration over E_a can be deducted setting the restriction for $| y_0 | \leq 1$:

$$E_a^{max} = \frac{E(m_a^2 + M^2 - m_b^2) + q\lambda^{1/2}}{2M^2} \text{ and } E_a^{min} = \frac{E(m_a^2 + M^2 - m_b^2) - q\lambda^{1/2}}{2M^2} \quad (C.17)$$

with $\lambda^{1/2} = \sqrt{(M^2 + m_a^2 - m_b^2)^2 - 4M^2 m_a^2}$ - usual triangle relation.

Hence the final expression for the differential rate for each particular type of interaction in the most general form is

$$E\frac{dR}{dM^2 d^3\vec{q}} = \mathcal{N} \int_{E_a^{min}}^{E_a^{max}} \int_{p_+^{min}}^{p_+^{max}} \frac{| \mathcal{M} |^2}{32(2\pi)^6 q^2} dp_+ dE_a f(E_a)\,(1 + f(E - E_a)). \quad (C.18)$$

where the limits of integration correspond to Equations C.12 and C.17.

Bibliography

[1] C. Wong, *Introduction to High-Energy Heavy-Ion Collisions* (World Scientific, Singapore, 1994).

[2] K. Kajantie, J. Kapusta, L. McLerran, and A. Mekjian, Phys.Rev. **D34**, 2746 (1986).

[3] E. Laermann, Nucl.Phys. **A610**, 1 (1996);

A. Peikert, F. Karsch, E. Laermann, B. Sturm, Nucl.Phys.Proc.Suppl. **73**, 468 (1999).

[4] P. Huovinen, P. V. Ruuskanen, J. Sollfrank, nucl-th/9807076.

[5] R. Albrecht *et al.*, Phys.Rev.Lett. **76**, 3506 (1996);

M. M. Aggarwal *et al.*, Phys.Rev.Lett. **81**, 4087 (1998);

M. M. Aggarwal *et al.*, Phys.Rev.Lett. **83**, 926 (1999);

M. M. Aggarwal *et al.*, Phys.Rev.Lett. **84**, 578(E) (2000).

[6] E. Scomparin *et al.* (NA50 collaboration), J.Phys. **G25**, 235 (1999);

P. Bordalo *et al.* (NA50 collaboration), Proc. of Quark Matter '99 (Torino, Italy, June 1999), to appear in Nucl.Phys. **A**;

M. C. Abreu *et al.*, Phys.Lett. **B410**, 337 (1997);

M. C. Abreu *et al.*, Phys.Lett. **B450**, 456 (1999);

M. C. Abreu *et al.*, CERN-EP-2000-013, submitted to Phys.Lett. **B**.

[7] G. Agakichiev *et al.*, Phys.Lett. **B 422**, 405 (1998);

B. Lenkeit *et al.*, Nucl.Phys. **A654**, 627c (1999);

B. Lenkeit *et al.*, Nucl.Phys. **A661**, 23c (1999);

P. Wurm for the CERES collaboration, Nucl.Phys. **A590**, 103c (1995).

[8] A. L. S. Angelis *et al.* (HELIOS-3 collaboration), Eur.Phys.J. **C5**, 63 (1998);

N. Masera for the HELIOS-3 collaboration, Nucl.Phys. **A590**, 93c (1995).

[9] F. Becattini, J. Cleymans, A. Keranen, E. Suhonen, K. Redlich, submitted to Phys.Lett. **B**, hep-ph/0002267.

[10] T. Alber *et al.*, Phys.Rev.Lett. **75**, 3814 (1995);

H. Appelshuser *et al.*, Eur.Phys.J. **C2**, 661 (1998);

F. Sikler *et al.*, Nucl.Phys. **A661**, 45c (1999).

[11] T. Matsui and H. Satz, Phys.Lett. **B178**, 416 (1986).

[12] T. Hatsuda *et al.*, Nucl.Phys. **A590**, 545c (1995).

[13] J. Rafelski *et al.*, Phys.Rev.Lett, **48**, 1066 (1982).

[14] P. V. Ruuskanen, Nucl.Phys. **A525**, 255c (1991).

[15] B. Lenkeit for the CERES collaboration, Proc. of Quark Matter '99, (Torino, Italy, June 1999), to appear in Nucl.Phys. **A**.

[16] E. V. Shuryak, Phys.Lett. **78B**, 150 (1978).

[17] R. Rapp and J. Wambach, Adv.Nucl.Phys. (in print), nucl-th/9909229.

[18] W. Cassing and E. L. Bratkovskaya, Phys.Rep. **308**, 65 (1999).

[19] G. E. Brown and M. Rho, Phys.Rev.Lett. **66**, 2720 (1991).

[20] R. Rapp, G. Chanfray, and J. Wambach, Nucl.Phys. **A 617**, 472 (1997).

[21] F. Klingl, N. Kaiser, and W. Weise, Nucl.Phys. **A 624**, 527 (1997).

[22] P. V. Ruuskanen, Nucl.Phys. **A544**, 169c (1992).

[23] E. V. Shuryak, Nucl.Phys. **A 533**, 761 (1991).

[24] R. Rapp and E. V. Shuryak, to appear in Phys.Lett. **B**, hep-ph/9909348.

[25] L. Xiong, E. Shuryak, and G. E. Brown, Phys.Rev. **D46**, 3798 (1992).

[26] Z. Huang, Phys.Lett. **B361**, 131 (1995).

[27] Ulf-G. Meissner, Phys.Rep. **161**, 213 (1988).

[28] K. L. Haglin and C. Gale, nucl-th/0010017.

[29] J. J. Sakurai, *Currents and Mesons* (The University of Chicago Press, Chicago,1969).

[30] C. Gale and P. Lichard, Phys.Rev. **D49**, 3338 (1994).

[31] R. Rapp and C. Gale, Phys.Rev. **C60**, 024903 (1999).

[32] C. Song, hep-ph/9603259.

[33] C. Gale, D. Seibert, and J. Kapusta, Phys.Rev. **D56**, 508 (1997).

[34] I. Kvasnikova and C. Gale, AIP Conf. Proc. 488, MRST '99, 214 (1999).

[35] C. Gale and J. Kapusta, Nucl.Phys. **B357**, 65 (1991).

[36] Particle Data Group, Phys.Rev. **D54**, (1996).

[37] K. Haglin, C. Gale, and V. Emel'yanov, Phys.Rev. **D47**, 973 (1993).

[38] S. Gao and C. Gale, Phys.Rev. **C57**, 254 (1998).

[39] C. Song, C. M. Ko and C. Gale, Phys.Rev. **D50**,1827 (1994).

[40] H. Gomm, O. Kaymakcalan, and J. Schechter, Phys.Rev. **D30**, 2345 (1984).

[41] B. A. Li, Phys.Rev. **D52**, 5165 (1995).

[42] V. Koch, Int.J.Mod.Phys. **E6**, 203 (1997).

[43] L. G. Landsberg, Phys.Rept. **128**, 301 (1985).

[44] J. W. Durso, Phys.Lett. **B184**, 348 (1987).

[45] D. Bisello *et al.*, Phys.Lett. **B220**, 321 (1989).

[46] N. Albrecht *et al.*, Phys.Lett. **B185**, 223 (1987).

[47] M. E. Biagini, S. Dubnicka, E. Etim, and P. Kolar, Nuovo Cimento, **A104**, 363 (1991).

[48] K. Haglin and C. Gale, Nucl.Phys. **B421**, 613 (1994).

[49] S. I. Dolinsky *et al.*, ND Collaboration, Phys.Rep. **202**, 99 (1991).

[50] N. Albrecht *et al.*, ARGUS Collaboration, Phys.Lett. **B185**, 223 (1987).

[51] D. Bisello *et al.*, DM2 collaboration, *Proceedings of hadrons 91*, College Park, 1991 (unpublished).

[52] G. Q. Li and C. Gale, Phys.Rev. **C58**, 2914 (1998).

[53] J. Cleymans, K. Redlich, and D. K. Srivastava, Phys.Rev. **B420**, 261 (1998).

[54] J. D. Bjorken, Phys.Rev. **D27**, 140 (1983).

[55] L. D. Landau and E. M. Lifshitz, *Fluid mechanics* (Pergamon, New York,1959).

[56] R. Venugopalan, M. Prakash, M. Kataja, and P. V. Ruuskanen, Nucl.Phys. **A566**, 473c (1994).

[57] U. Ornik, F. W. Pottag, and R. M. Weiner, Phys.Rev.Lett. **63**, 2641 (1989).

[58] E. Schnedermann and U. Heinz, Phys.Rev.Lett. **69**, 2908 (1992);
E. Schnedermann, J. Sollfrank, and U. Heinz, Phys.Rev. **C48**, 2468 (1994).

[59] J. Bolz, U. Ornik, and R. M. Weiner, Phys.Rev. **C46**, 2047 (1992).

[60] U. Katscher *et al.*, Z.Phys. **A346**, 209 (1993).

[61] J. Cleymans, K. Redlich, and D. K. Srivastava, Phys.Rev. **C55**, 1431 (1997).

[62] J. Sollfrank, P. Huovinen, M. Kataja, P. V. Ruuskanen, R. Venugopalan, M. Prakash, Phys.Rev. **C55**, 392 (1997).

[63] S. A. Bass, A. Dumitru, Phys.Rev. **C61**, 064909 (2000).

[64] I. Kvasnikova, C. Gale, D. K. Srivastava, and B. Sinha, in preparation.

[65] D. K. Srivastava, B. Sinha, and C. Gale, Phys.Rev. **C53**, R567 (1996).

[66] P. L. McGaughey et al, Phys.Rev. **D50**, 3038 (1994).

[67] J. F. Owens and Wu-Ki Tung, Ann.Rev.Nucl.Part.Sci. **42**, 291 (1992).

[68] M. Gluck, E. Reya, and A. Vogt, Z.Phys. **C67**, 433 (1995).

[69] M. C. Abreu *et al.*, NA38 and NA50 Collaborations, Eur.Phys.J.C **14/3**, 443 (2000).

[70] X. N. Wang, Phys.Rept. **280**, 287 (1997).

[71] E. V. Shuryak, Phys.Rep. **61**, 71 (1980).

[72] P. V. Ruuskanen, in *Quark-Gluon Plasma*, edited by R. Hwa, (World Scientific, Singapore 1990), p.519.

[73] K. Gallmeister, B. Kämpfer and O. P. Pavlenko, hep-ph/9809318.

[74] N. Isgur, C. Morningstar, and C. Reader, Phys.Rev. **D39**, 1357 (1989).